Contemporary systematics of vadose zone nitrate capture by speleothem carbonate

Wynn P.M[a*]., Ambler, S[a]., Grefe I[a]., Soto D.X[b]., Surridge, B.W.J[a]., Gabitov, R.I[c]., Barker, P.A[a]., Anwar, J[a]., Quin, A[a]., Pereira, M.G[b]. and Grant H.K[b]

[a]*Lancaster Environment Centre, Lancaster University, Lancaster, LA1 4YQ, UK.*

[b] UK Centre for Ecology and Hydrology, Lancaster, LA1 4AP, UK

[c]*Department of Geosciences, Mississippi State University, Mississippi State,* MS 39762, United States.

* Corresponding author. E-mail address: p.wynn@lancaster.ac.uk

Abstract

The movement of nitrate through the vadose zone has major implications for environmental and human health. This issue is particularly prevalent in karst terrain where agricultural activity, thin soils and dual permeability compound the problem of high nitrate loading to the overlying ecosystem. However, a paucity of records which document vadose zone nitrate concentrations prior to the 21st century render legacy nitrate dynamics, source attribution and baseline conditions to be poorly parameterised. Speleothems growing within karst cave settings may provide an opportunity to obtain records of vadose zone nitrate contamination which extend throughout the anthropogenic era. Here, we use dual isotope analysis of $\delta^{15}N_{NO_3}$ and $\delta^{18}O_{NO_3}$ in a contemporary study at Cueva-cubío del Llaníο, N. Spain, designed to examine the transformation of nitrate between surface to cave environment, taking account of biogeochemical transformation, karst hydrology and partitioning as controls on the delivery of nitrate to the speleothem record. Concentrations of nitrate within speleothem calcite are low (measured range of 0.05mM to 0.37mM) due to partitioning (D_{NO_3}) across the dripwater-calcite interface. Values of $\delta^{15}N_{NO_3}$ extracted from cave waters in Cueva-cubío del Llaníο (range +2.0 to +7.0‰) are shown to be excellent indicators of nitrate source and demonstrate no fractionation during incorporation into speleothem carbonate (range of $\delta^{15}N_{NO_3}$ in speleothem carbonate +1.6‰ to +6.4‰). Values of $\delta^{18}O_{NO_3}$ contained within cave waters (range -2.5‰ to +6.0‰) and speleothem carbonate (range +12.3‰ to +32.3‰) reflect a mixed signal of source, biogeochemical processing and hydrological pathway, providing critical insight into the behaviour of the karst aquifer. Contemporary systematics at Cueva-cubío del Llaníο therefore confirm speleothem carbonate contains an excellent record of vadose zone nitrate. Analysis of nitrate contained within speleothem carbonate from other regions confirms the ubiquitous nature of partitioning across the water-carbonate interface and the use of speleothem nitrate isotopes for recording surface ecosystem processes and vadose zone behaviour. Application of these principles to dated speleothem records should provide critical timeseries of nitrate loading, enabling understanding and remediation against the presence of vadose zone legacy nitrate.

1. Introduction

Loading of reactive nitrogen to the global biogeochemical cycle is impacted heavily by anthropogenic activity. Industrial pollution releases nitrogen compounds into the atmosphere, and intensification of agricultural practices exacerbates the input of reactive nitrogen to the biosphere through the application of organic materials and inorganic fertilisers. The resultant fluxes of reactive nitrogen can adversely affect freshwater ecosystems through eutrophication and acidification, as well as impact human health through nitrate contamination of groundwater used for drinking water supplies (eg. Vitousek, 199; Galloway et al., 2008; Matiatos et al., 2021). However, the loss of reactive nitrogen to the vadose zone, where leaching from surface to groundwater and slow transit times leads to the longterm storage of nitrate is poorly quantified (Ascott et al., 2017). Retention of nitrate in the vadose zone has created a 'nitrate time bomb', whereby the impact of peak N application has been delayed to create a problem for future generations (Wang et al., 2013). Despite recent controls on anthropogenic nitrogen loading in some countries, many environmental systems will continue to suffer from 'legacy nitrate' on a timescale which depends upon the storage and release dynamics of vadose systems. This is particularly the case for karstic bedrock which forms a significant proportion of the global vadose zone, with over a quarter of the World's population relying on water sourced from karst regions (Ford and Williams, 2013). Karst systems present a unique hydraulic configuration, comprising dual permeability characteristics of rapid fracture and slow matrix flow. Thin soils and fracture pathways convey surface pollution rapidly into the vadose system, making them acutely vulnerable to contamination, whilst the remaining pollutant load can become entrapped within the matrix porosity of the carbonate bedrock, forming a significant store of legacy nitrate within the vadose zone. However, whilst empirical observations of karst vadose zone nitrate dynamics are reasonably well studied over event based to decadal time scales (eg. Jiménez-Sánchez et al., 2008; Husic et al., 2019a,b and compilation of references therein; Yue et al., 2018; Yue et al., 2019; Yang et al., 2020), observations prior to 21st century monitoring are rare. This leaves a lack of knowledge regarding baseline pre-industrial vadose zone nitrate concentrations, no information on changing nitrate sources prior to the 21st century and no empirically determined rates of nitrate

transfer through the dual permeability karst vadose zone system. Where nitrogen biogeochemical cycling can be traced through the soil-karst system using stable isotopes, and the incorporation of nitrogen species into calcium carbonate can be parametrised, speleothems (cave stalagmites and stalactites) growing in karst regions could be used to overcome this lack of knowledge, providing a natural, time-resolved archive of vadose zone nitrate dynamics. Stalagmites growing in cave environments incorporate trace elements and nutrients delivered from the overlying vadose zone of karst storage, via drip waters. The drip water record will therefore be incorporated into speleothem calcite reflecting surface loading and the lag time associated with vadose zone storage. The nitrogen content of speleothem calcite which has grown consistently throughout the past ~200 years could ultimately enable contextualisation of surface nitrogen loading, recording time-bomb type waves of nitrate passing through the vadose zone prior to entering the deeper groundwater system. However, the linkage between groundwater legacy nitrate and the speleothem record initially needs to take into account biogeochemical modification of surface inputs, karst transfer and partitioning into contemporary carbonate deposits. Here, we use stable isotopes to trace the movement of nitrate between surface pasture ecosystem to cave drip waters and associated contemporary speleothem deposits. We specifically address the ability of contemporary speleothem carbonate to accurately represent the chemical and isotopic signature of dripwater nitrate, thereby unlocking the potential for stalagmites which have grown throughout the 19th to 20th centuries to provide a time-resolved record of vadose zone nitrate dynamics.

2. Karst nitrogen biogeochemical cycling and transfer into carbonate

2.1. Nitrogen biogeochemical pathways in karst ecosystems

Biogeochemical modification of surface inputs serve to control the entry of nitrate into the vadose zone, potentially also modifying isotopic signatures away from source values. Biogeochemical cycling of nitrogen typically consists of five key processes 1. Nitrogen fixation (bacterial fixing of atmospheric N_2 into the organic phase), 2. Mineralisation and nitrification (representing the overall conversion of organic N to ammonia and then to nitrate within the soil/root zone), 3. Assimilation (uptake of soil ammonia and nitrate into the organic phase), 4. Volatilisation (vaporisation of ammonia compounds from the soil surface in the aftermath of application) and 5. Denitrification (the conversion of oxidized nitrogen compounds to N_2 gas under conditions of low oxygen status).

Nitrogen fixation causes only limited nitrogen isotope fractionation (-2 to +2‰) (Casciotti, 2009 and references therein), and denitrification would not be expected to play a large role in the karst biogeochemical nitrogen cycle due to limited potential for the development of anoxia within the karst vadose zone and overlying soils. The three main fractionating processes of concern to karst environments are therefore volatilisation, assimilation and nitrification. The extent to which these biogeochemical processes modify source signatures away from recognisable end-member isotopic values is dependent upon site-specific antecedent conditions controlling the degree of fractionation inherent in each.

Volatilisation is known to cause extensive loss of ammonia to the atmosphere (Cameron et al., 2013) and equilibrium isotopic fractionation during volatilisation is documented as approximately +30‰, thereby enhancing the residual soil ammonium pool in ^{15}N (Heaton, 1986). However, in karst ecosystems dominated by pasture grazing and which are replete in nitrogen, there is reportedly limited potential for this enriched signature to be translated directly into nitrate leachates due to overprinting of the residual ammonium isotopic signature by soil mineralisation and nitrification (Wells et al., 2015).

Fractionation during assimilation causes ^{15}N depletion in plant-based tissues relative to the substrate isotopic composition. Measured fractionation varies between 0‰ to +12.6‰ for net ammonia assimilation into plants (Evans, 2001 and references therein) and 0‰ to +18‰ for net nitrate assimilation into plants under open system conditions (Liu et al., 2014 and references therein; Evans, 2001 and references therein), thus generating a residual soil pool enriched in ^{15}N. However, the impact of assimilation and associated kinetic fractionation upon the soil N pool is largely dependent upon whether the soil system is representative of an open or closed system. In an open system where soil N supply continuously exceeds demand, fractionation will produce an offset between plant and

soil, although the soil isotopic composition will not change over time. Under closed or semi-closed system conditions where soil N supply cannot always satisfy demand, substrate concentration will decline through time. Both soil substrate and plant N will gradually become enriched in ^{15}N and assimilated plant N will converge on the initial soil substrate isotopic composition. Karst ecosystems supporting an agricultural land use are replete in nitrogen and likely follow the principles of an open system, such that assimilative activity has little effect upon soil nitrogen isotopic status. However, karst ecosystems supporting natural vegetation are more likely to be nitrogen limited, thus causing temporal variation in the soil substrate isotopic composition. The open/closed nature of a karst system will also be dependent upon the seasonality of plant demand for nitrogen.

The overall conversion of organic-N to nitrate comprises mineralisation (the conversion of organic N to ammonia) and nitrification (the oxidation of ammonia to nitrate). Mineralisation rarely causes fractionation (eg. Heaton et al., 1986; Högberg, 1997). However, the nitrification of ammonium to nitrite causes a kinetic fractionation to $\delta^{15}N$ which ranges between +24.6‰ to +38.2‰ based on terrestrial strains of ammonia oxidizing bacteria (*Nitrosospira tenuis, Nitrosomonas eutropha, and Nitrosomonas europaea*) (Casciotti et al., 2003 and references therein). The conversion of nitrite to nitrate is associated with an inverse isotopic fractionation of -12.8 +/- 1.5‰ (*Nitrococcus mobilis,* Casciotti, 2009). The overall fractionation for the entire nitrification pathway is dependent upon environmental conditions and the relative dominance of substrate pool size. Where the system is nitrogen limited, the rate-determining step is represented through the mineralisation of organic-N to ammonia. As mineralisation supports limited fractionation, the $\delta^{15}N$ of product nitrate will closely resemble the isotopic composition of the total organic nitrogen (Heaton et al., 1986). However, where the substrate ammonium is in abundant supply, initial oxidation products may be expected to be isotopically depleted in ^{15}N. As the ammonium substrate pool becomes depleted in abundance, isotopic fractionation should approach unity, such that nitrate oxidation products are of similar isotopic value to initial ammonium signatures. In karst systems supporting agricultural activity, nitrogen availability should be replete and product soil water should be isotopically depleted compared to source. For those karst systems which are not impacted by agriculture, soil water nitrate will be representative of N source. During nitrification, the stoichiometric incorporation of oxygen into the nitrate molecule comprises a maximum 1:2 ratio of oxygen sourced from O_2 and H_2O, although discrepancies to this theoretical rule may be expected in natural systems (eg. Mayer et al., 2001 ; Venkiteswaran et al., 2019 ; Romanelli et al., 2020). The oxidation of ammonia to nitrite utilises oxygen from O_2 and H_2O in equal proportions, but also encompasses an isotopic fractionation to $\delta^{18}O$ during the incorporation of each which can be collectively parameterised as +19.3+/-2.9‰ (bacterial strain *Nitrosomonas europaea*) or +30.3 +/-1.0‰ (bacterial strain *Nitrosospira briensis*, Casciotti et al., 2010). The exchange of oxygen between nitrite and water also has the effect of causing an equilibrium isotopic fractionation of approximately +14‰ (Casciotti et al., 2007). The oxidation of nitrite to nitrate incorporates one oxygen atom sourced from water into the nitrite molecule (isotopic fractionation parameterised as +12.8‰ to +18.2‰, Buchwald and Casciotti, 2010). Fractionation also occurs at the point of nitrite oxidation, and during oxygen atom exchange with water although these two sources are noted to be minimal under oxidizing conditions where nitrite availability is low (Buchwald and Casciotti, 2010). Within karst systems where nitrate is sourced as a product of nitrification, values of $\delta^{18}O_{NO_3}$ will therefore lie between a defined upper and lower threshold dependent upon the water-oxygen isotopic composition and the range of fractionation factors employed.

The overall impact of biogeochemical cycling and fractionation in karst systems thus depends upon whether the system is considered open or closed, and replete or limited in nitrogen. Where karst systems are nitrogen limited and predominantly closed to excessive new inputs, volatilisation will be limited, assimilation will progress towards completion and the nitrification pathway will be controlled by mineralisation, causing minimal fractionation to $\delta^{15}N_{NO_3}$. Nitrate isotopic signatures entering into the vadose zone will thus reflect those of surface inputs, with an expressed seasonality in $\delta^{18}O_{NO_3}$ dependent upon the relative significance of nitrifying activity. However, where karst soils support agricultural activities, the system must be considered open and replete in nitrogen. Volatilisation will be extensive, although any associated isotopic fractionation will be largely overprinted by the nitrification pathway. Assimilation will have limited effect on the isotopic composition of the soil substrate N pool. Under this scenario, nitrate isotope values present in cave drip waters will likely be depleted in ^{15}N compared to source signatures. Both $\delta^{15}N_{NO_3}$ and $\delta^{18}O_{NO_3}$ may express pronounced seasonality dependent upon the extent of nitrification occurring within the soil zone.

2.2 Transfer of nitrate through karst and into speleothem carbonate

The complex drainage structure of karst systems serves to modify isotopic signatures of nitrogen biogeochemical cycling away from those identified at the base of the soil zone. The dual permeability of karst bedrock comprises a rapid fracture flow and a slow matrix flow system. Whereas the fracture system is ephemeral, matrix systems fill during times of water excess to deliver a steady water flux over a prolonged period of time. Where rapid fracture flow is the dominant hydrological pathway, water demonstrates little storage or mixing within the karst. Water can be of meteoric origin or from the soil zone, with associated nutrient signatures being routed through the karst with such rapidity as to obviate any isotopic differences due to vadose zone processes (eg. Wynn et al., 2013). However, within the slow matrix flow system, storage and mixing can occur across multiple timescales to create a nitrogen signal which reflects a homogenisation of sources and biogeochemical processes, otherwise known as legacy nitrate. Soil waters charged with carbonic acid will also come into prolonged contact with carbonate bedrocks, and dissolution of the host bedrock will release constituent trace ions into solution. This bedrock end member may contribute sufficient N to control the composition of the dripwater solution if nitrogen concentrations are high and/or support an isotopic value which is distinctly different to the aqueous solution. An upper estimate of nitrogen contribution from bedrock dissolution can be calculated as follows $^{\%\ bedrock}NO_3 = [1/(^{bedrock}Ca+Mg{:}NO_3/^{dripwater}Ca+Mg)/^{dripwater}NO_3] \times 100$. This equation is based on Wynn et al., 2008, assuming only limited contributions of calcium and magnesium from extraneous sources such as rainfall, plant necromass and organic fertilisers, alongside limited impact of prior calcite precipitation upon drip water ratios to nitrate). Where a component of slow matrix flow contributes to the hydrological regime, the biogeochemical signature conveyed in cave drip waters is therefore not a direct reflection of source (atmospheric deposition or soil zone biogeochemistry), but also represents hydrological pathway, time-integrated storage dynamics, and additional inputs from bedrock dissolution.

When cave drip waters actively deposit calcium carbonate onto speleothem growth surfaces, the nitrate ion can become incorporated into the calcite (Kontrec et al., 2004). The incorporation mechanism, however, remains unresolved. Partition co-efficients of the form $DNO_3 = (NO_3/CO_{3solid})/(NO_3/CO_{3solution})$ have also yet to be established (cf. Wynn et al., 2018) and associated controls on incorporation identified through controlled calcite growth experiments. Any degree of isotopic fractionation across the aqueous-solid interface is also in need of parameterisation. The bulk nitrate signature conveyed within cave drip waters comprising source signature, soil biogeochemical processing, bedrock dissolution, karst attenuation and mixing, will thus be incorporated into speleothem calcite at a temporal resolution dependent upon growth rate. Where isotopic signatures can be deconvolved according to the above framework of biogeochemical cycling and phase boundary partitioning, information on changes in nitrogen source can be obtained. Time-resolved changes in speleothem concentration dynamics can be used to determine vadose zone storage and thus legacy effects within karst landscapes, as well as pre-anthropogenic baseline status. Speleothems could thus become one of the most significant archives of legacy nitrate dynamics, providing a record of sufficient longevity for the improvement and testing of existing empirical groundwater models.

3. Methodology

3.1 Cave site description and sample collection regime

Cueva-cubío del Llanío is a shallow cave system located within the Cantabrian Cordillera of N. Spain (43°21’29.9”N, 003°35’53.8”W, 165 m a.s.l). It is located within the Riaño valley, 21 km south east of Santander, forming part of a connected network of caves which link to those of the neighbouring Matienzo depression (eg. Smith et al., 2015, 2016a,b). The cave is developed in Lower Cretaceous (Aptian-Albian) carbonate of shallow water platform origin (Dewitt et al., 2014; Aranburu et al., 2015), with host bedrock comprising a mixed calcite-dolomite composition (70% dolomite content calculated following Fairchild and Treble, 2009), interbedded with sandstones and marl (Gutiérrez, 2010). The soil is organic rich and with loamy texture, often in excess of 50 cm depth, supporting a clover-rich pasture of variable grazing intensity. Cave drip waters were sampled on a seasonal

basis from two chambers which supported contrasting surface vegetation characteristics (Figure 1). High Hopes chamber was located at a depth of approx. 14 m beneath managed pastureland formerly fertilised with manure (manure application ceased in 2017), whereas Whoopee Hall was located at a shallower depth of approx. 5 m beneath steeply sloping pasture with low intensity grazing and minimal manure application.

Drip sites in High Hopes chamber support a range of hydrological characteristics. High Hopes drips 1-6 are delivered via soda straw stalactites and feed actively depositing speleothems. Each drip is predominantly matrix fed, albeit with flow recession during the summer months reflecting the seasonality of rainfall dynamics within the region (eg. Smith et al., 2016b). Drip water discharges range between 64 ml to 598 ml per day, with greatest sensitivity to rainfall events being observed during the winter season (see drip logger record for High Hopes 2 and 3 in Figure S1). Fast drips 1 and 2 are located approx. 5 meters away within the same chamber, albeit represent a more ephemeral flow of water entering into the cave and are likely to be at least partially fracture fed. The drip site in Whoopee Hall delivers dripwater from a soda straw stalactite onto an actively growing stalagmite. Dripwater discharge is up to 711 ml per day. A persistent winter discharge, albeit with flow cessation during the summer months at this site is suggestive of a predominantly matrix fed hydrology, albeit from a reservoir of sufficiently limited volume to prevent year-round flow characteristics (see drip logger record for Whoopee Hall in Figure S1). Pool waters within both chambers were fed by the ephemeral, fracture flow drip sites.

Each drip site was sampled over a time interval commensurate with discharge characteristics. For those sites where water flow was sufficient, samples were collected instantaneously during a typical 4-hour period within the cave. Drip site High Hopes 1 supported a sufficiently slow drip rate to enable sample collection only on seasonally scheduled visits to the cave. All other drip sites had water samples collected over a 24-hour period. Pool waters within the cave were ephemeral and thus sampled whenever possible during scheduled cave visits. After drip and pool water collection, samples were tested for pH, EC (electrical conductivity) and temperature. One aliquot of each sample (approx. 30 ml) was filtered through a 0.2 micron membrane (polyethersulfone) filter and stored frozen (-20°C) within a Nalgene LDPE bottle. Any remaining water up to a maximum of 60 ml was stored unfiltered and refrigerated prior to further analysis. Rainfall dynamics were monitored in the neighbouring village of Matienzo using a Pluvimate drip logger (Driptych.com) to record both rainfall intensity and volume (see record provided in Figure S1). Rainfall was also collected for nitrate isotopic analysis as monthly bulk collections on an ad-hoc basis. Soil and vegetation samples were collected from above the cave to monitor nitrogen content and isotopic composition. Soil samples were collected as composite cores up to 10 cm in depth, and vegetation samples were collected from the same locations. Sediment samples were collected from within the cave system to represent an integrated sample of inwashed material and cave internal breakdown products.

Modern speleothem calcite was grown on either glass plates (up-turned watch-glasses pre-cleaned using an acid wash, no etching used to encourage calcite nucleation) or stalagmate logger surfaces placed beneath each of the drip sites defined above, and left to deposit for approximately 6 months between collections. Upon removal from the cave, the calcite deposit was removed using a scalpel. Samples were homogenised and stored prior to analysis for nitrate concentration and isotopic composition. Archived speleothem samples were used to expand the speleothem nitrate data set to cave sites with differing vegetation characteristics and nitrogen inputs. These sites comprised stalagmites collected from Rukiesa Cave, Ethiopia (Asrat et al., 2007, 2008; Baker et al., 2007), Browns Folly Mine, Somerset, UK (Baker et al., 1998, 1999a; Baldini et al., 2001, 2005; Fairchild et al., 2006), and Ease Gill Cavern, Cumbria. Calcite grown on glass plates in Cueva de las Perlas, Matienzo, N. Spain (Deeprose, 2018) and Pooles Cavern, Buxton, UK (Baker et al., 1999b; Baker and Genty, 1999; Hartland et al., 2010, 2011, 2012; Newton et al., 2015) were also utilised for nitrate extraction. Carbonate powders which represented the most recent speleothem growth prior to collection were extracted from all samples other than Ease Gill Cavern. At this latter site, the fossil nature of the speleothem provided an opportunity to obtain a pre-anthropogenic sample.

3.2 Laboratory methodology

Nitrate concentrations in cave dripwater, pools and rainfall, were analysed from the filtered water aliquot using automated colourimetry (SEAL AQ2 analyser), based on the cadmium reduction of nitrate to nitrite with an analytical range of 0.06 to 5 mg l^{-1} NO_3-N and a limit of detection (LOD) of 0.01 mg l^{-1} NO_3-N. Concentrations were not corrected for the presence of nitrite, due to it being below the range of the AQ2 analyser within a representative subset of samples (analytical range of 0.01 to 0.1 mg l^{-1} NO_2-N). Concentrations of ammonia were determined on the same sample aliquots by SEAL AQ2 analyser, based on indophenol blue colourimetry and with an analytical range between 0.02 to 2 mg l^{-1} NH_4-N. For both techniques analytical precision based on the repeat analysis of reference standard material (0.25 mg l^{-1} and 1 mg l^{-1} N for both nitrate and ammonia analysis) is reported to within 5% of expected values. The total carbonate composition of aqueous samples was determined using titration with phenolphthalein and Bromocresol indicators. The cation composition of cave waters (Ca, Mg) was analysed by Inductively Coupled Plasma Optical Emission Spectroscopy (ICP-OES), at Lancaster University, UK, using a Thermo Scientific iCAP 6000. Each sample was acidified using ultrapure nitric acid to achieve a final concentration of 0.1M, matrix matched to standard solutions. Repeat analysis of reference standard material (concentration of 1 mg l^{-1} for all species analysed) is reported to within 5% of expected values.

Nitrate isotope analysis was undertaken on drip water samples using the microbial denitrifier technique (Sigman et al., 2001; Casciotti et al., 2002) at the Lancaster Environment Centre, Lancaster University, UK. This technique used cultures of *Pseudomonas chlororaphis*, a denitrifying bacterium lacking nitrous oxide reductase, to convert 20 nmol of sample nitrate to nitrous oxide. Speleothem and bedrock carbonates were also analysed for nitrate isotopic content using the microbial denitrifier technique. Sufficient speleothem powder (typically 100 mg) was dissolved stoichiometrically in ultrapure 1M hydrochloric acid to a neutral pH. The reaction was undertaken at room temperature to prevent any oxygen isotopic exchange between nitrate and water under low pH (Kaneko and Poulson, 2013). After carbonate dissolution, the digestate was diluted to 5 ml with de-ionised water and the whole sample injected into 20 mL headspace vials containing the bacterial cell suspension. For both drip waters and carbonates, the headspace nitrous oxide was subsequently injected into an Isoprime Trace gas preconcentrator inlet and autosampler, coupled to an Isoprime Isotope ratio Mass Spectrometer (IRMS) at the NERC National Environmental Isotope Facility (NEIF) at CEH Lancaster, UK. International reference materials (USGS-34, USGS-35 and IAEA-NO-3) were used for calibration, assuming $\delta^{15}N$ values of -1.8‰ and +4.7‰ for USGS 34 and IAEA-NO-3, and $\delta^{18}O$ values of -27.9‰, +57.5‰ and +25.6‰ for USGS-34, USGS-35 and IAEA-NO-3 respectively. Within-run standard precision for both international and in-house standards was <0.2‰ and <0.5‰ (1SD) for $\delta^{15}N_{NO_3}$ and $\delta^{18}O_{NO_3}$ respectively. Triplicate analysis of selected samples in each run sequence (both cave waters and speleothem digests) yielded sample analytical precision within the same range. Background contamination (analysis of microbial culture without sample inoculation) averaged 0.7% (range 0.5% to 1.4%) of the in-house standard peak area. To test for matrix effects during speleothem nitrate isotopic analysis, a carbonate with low nitrate content was digested following the protocol above and spiked with the in-house standard prior to analysis with the denitrifier method. $\delta^{15}N_{NO_3}$ and $\delta^{18}O_{NO_3}$ values were within error (1SD precision) of values expected for the internal standard, showing no discernible matrix effects from the acid digest. The nitrate concentration contained within each cave water, speleothem and bedrock carbonate analysis was determined by peak area integration using IonVantage software.

Determination of total nitrogen content and isotopic composition within vegetation, sediment and soil samples was undertaken at the Lancaster Environment Centre stable isotope laboratory, Lancaster University using an Elementar varioMICRO elemental analyser interfaced to an Isoprime 100 continuous-flow isotope ratio mass-spectrometer. Vegetation samples were dried at 50 °C for 24 hours, crushed and homogenised. Sediment and soil samples were dried at 50 °C for 48 hours, sieved to remove any large rock fragments and subsequently crushed. Combustion of samples within tin capsules at 950 °C yielded N_2 for analysis of $\delta^{15}N_{total}$. Within-run replication of international and in-house standards was better than 0.3‰ (1SD) for $\delta^{15}N$. Concentrations of total nitrogen were calculated using peak area integration in the varioMICRO software, calibrated to within-run determinations of acetanilide.

3.3 Mixing models

A Bayesian isotope mixing model (MixSIAR operated in open-source R software, Stock and Semmens, 2013) was used to determine the relative proportion of nitrate sources (e.g. Soto et al. 2019) in cave waters and contemporary speleothem calcite. The end-member sources for dissolved nitrates used to drive the model comprised (1) manure (+13.0 ± 4.3 for $\delta^{15}N$ and -8.45 ± 2.20 for $\delta^{18}O$), (2) precipitation (+1.00 ± 1.64 for $\delta^{15}N$ and +66.48 ± 3.67 for $\delta^{18}O$), and (3) NO_3 derived from the nitrification of rainfall NH_4^+ and re-mineralisation of fixed N_2 (-2.5 ± 2.50for $\delta^{15}N$ and -8.45 ± 2.20 for $\delta^{18}O$). The nitrogen and oxygen isotopic composition of precipitation nitrate was determined from samples collected in the study area. The $\delta^{15}N$ values for (1) and (3) were taken from the literature (Kendall et al. 2007, Chalk et al. 2019) and $\delta^{18}O$ values were estimated based on the range of expected values for theoretical nitrification in the system (calculated to range between -15.0‰ to -1.9‰). Inorganic fertilizers are not used in the pastures above the cave, therefore this nitrate source was not considered. We assumed that after conversion of inputs to nitrate, mixing below the soil zone occurred conservatively and further fractionation through biogeochemical cycling was deemed negligible. As nitrate isotopic signatures sourced from the re-mineralisation and nitrification of fixed N_2 cannot be isotopically distinguished from the nitrification of rainfall ammonium, these two inputs were considered as a single source in the model. For each type of material, a Bayesian mixing model was run with three chains of 300,000 iterations, a burn-in of 200,000 and a thinning of 100; including 'cave chamber' and 'water type' as fixed variables. All cave waters and contemporary speleothem calcite samples fall inside the mixing polygon formed by the sources.

4. Results

Concentrations of nitrogen and $\delta^{15}N_{NO_3}$ values for all measured aqueous (cave waters and rainfall), soil / sediment and vegetation samples are compiled and presented within Table 1 (full underlying dataset available through the data repository at http://dx.doi.org/10.17635/lancaster/researchdata/xxx). Rainfall forms the most dilute end member component of the system (arithmetic average rainfall concentration = 0.01 mM NO_3-N). The soils above the cave and sediments within the cave support concentrations of total nitrogen ranging between 35.7 to 461.9 mM (per kg) and vegetation growing immediately above High Hopes chamber contains the greatest total nitrogen content of all measured components (range 1555.3 to 2599.0 mM, per kg) (Table 1). Cave water nitrate concentrations plot intermediate to the rainfall and soil/sediment end-members (Figure 2). Ammonia-nitrogen is present within rainfall at low concentrations (average 0.012 mM, range 0.006 mM to 0.021 mM). In cave waters ammonia-nitrogen is present on just three separate sampling occasions, with inconsistent presence across drip sites (average 0.006 mM, range 0.002 mM to 0.017 mM). On all other occasions, ammonia-nitrogen in drip and pool waters is below detection.

Values of $\delta^{15}N_{NO_3}$ show clear distinction between rainfall and soil/sediment sources, such that rainfall forms the lightest isotopic end member (arithmetic average +1.0‰, range -1.3‰ to +3.0‰), compared to soils and sediments (average +5.2‰, range +2.3‰ to +8.0‰). Cave drip and pool waters support $\delta^{15}N_{NO_3}$ signatures that are similar in composition to the soils/sediments (average +5.5‰, range +2.0‰ to +7.0‰) (Figure 2). There is an isotopic shift in $\delta^{15}N_{NO_3}$ between the two cave chambers with waters in High Hopes chamber appearing more enriched in ^{15}N than those in Whoopee Hall (Figure 3). Whereas bedrock samples collected from within the cave demonstrate similar isotopic composition to the drip and pool waters (bedrock average $\delta^{15}N_{NO_3}$ = +4.5‰), bedrock dissolution is calculated to comprise an upper estimated contribution of 0.24% of the dripwater NO_3 (calculated using ratios of calcium + magnesium to nitrate following methods in Wynn et al., 2008), confirming minimal impact on drip water isotopic signature. The $\delta^{15}N$ composition of vegetation growing above the cave ranges between -1.1‰ to +2.3‰ (Table 1). Whilst $\delta^{18}O_{NO_3}$ values of rainfall range between +62.3‰ to +71.9‰, a distinct shift in isotopic signature is apparent between rainfall and cave waters (Figure 3), with cave water $\delta^{18}O_{NO_3}$ composition ranging between -2.5‰ to +6.0‰.

Nitrogen concentrations and isotopic compositions have also been measured from modern speleothem carbonate grown within each cave chamber at Cueva-cubío del Llanío (Table 2). Concentrations of nitrate range

between 0.05 to 0.37 mM NO_3. The relative efficiency of nitrate partitioning between drip waters and speleothem calcite ($DNO_3^{x\,10\text{-}5}$) is quantified as ranging between 0.06 to 0.42 across both cave chambers when substituting for carbonate (Table 2). On average, $\delta^{15}N_{NO_3}$ signatures in contemporary speleothem calcite (average +4.5‰, range +1.6‰ to +6.4‰) are enriched compared to those in the input rainfall (average +1.0‰, range -1.3‰ to +3.0‰), but show no difference in value compared to the source cave waters. The $\delta^{18}O_{NO_3}$ composition of modern carbonate lies between rainfall and cave water signatures (Figure 3). Analysis of nitrate concentration and isotopic composition is also extended to speleothems sourced from cave sites in other regions (Figure 4). Nitrate concentration shows a wide range in values from 0.02 to 0.86 mM NO_3, dependent on speleothem growth setting (Table 3). Where coeval drip water and speleothem chemistry have been obtained, this extends the range of $DNO_3^{x10\text{-}5}$ up to the value of 1.43 (Table 2). The range in speleothem $\delta^{15}N_{NO_3}$ is narrow (range +2.1 to +6.0‰), reflecting the restricted range in $\delta^{15}N$ composition from source materials (Table 3). However, the $\delta^{18}O_{NO_3}$ isotopic composition extends from +6.0‰ to +58.6‰, representative of end member materials and the extensive fractionating effects endured through biogeochemical cycling.

5. Discussion

Interpreting groundwater nitrate dynamics from speleothem calcite requires understanding of source signatures, biogeochemical cycling and hydrological routing through karst. Isotopic fractionation adjusts signatures from source composition and partitioning of nitrate between water and calcite will offset speleothem concentration profiles from true groundwater characteristics. Here, we use knowledge from the fields of nitrogen biogeochemical cycling, groundwater hydrology and carbonate chemistry, to trace the evolution of nitrogen inputs from source to speleothem. We use this to build an appreciation for the potential of age-constrained speleothem records to provide an archive of groundwater nitrate dynamics.

5.1 The nitrate composition of cave dripwaters

The nitrogen biogeochemical cycle at Cueva-cubío del Llanío is known to comprise three main inputs: rainfall, manure-derived nitrogen and nitrogen fixation. The absence of inorganic fertiliser addition to the pastureland above the cave site precludes this source as a contributor to the drip water nitrogen signal. These inputs can be expected to support end member isotopic compositions in the following range: Atmospheric wet deposition $\delta^{15}N_{NO_3}$ and $\delta^{15}N_{NH_4}$ = -15‰ to + 15‰ (Kendall et al., 2007), $\delta^{18}O_{NO_3}$ ~ +60‰ to +95‰ (Kendall et al. 2007); Manure-derived $\delta^{15}N_{total}$ = -2.8‰ to +45.2‰ (Chalk et al., 2019 and references therein); Fixed N_2 ($\delta^{15}N_{fixation}$) = 0‰ +/- 2‰ (Casciotti, 2009 and references therein). The cave drip water nitrate composition reflects this balance of inputs, albeit tempered by biogeochemical processes comprising ammonia volatilisation, assimilation into the organic phase, soil mineralisation and nitrification. The inorganic dissolution of karst bedrock within the vadose zone and physical processes of hydrological mixing and storage will also cause the dripwater nitrate composition to deviate from input signatures.

Concentrations of nitrate within cave drip and pool waters are elevated relative to input rainfall. Element ratios to chloride and $\delta^{18}O/D_{H_2O}$ isotopic signatures from other cave sites within the region have indicated the majority of cave water recharge to be restricted to the winter season and the effects of evapocentration on cave drip water chemistry to be limited (Smith et al., 2016b; Deeprose, 2018). Translating the assumption of limited evapo-concentration affecting cave drip water chemistry to Cueva-cubío del Llanío, alongside a limited input of N from bedrock dissolution, dripwater nitrogen composition appears to be a product of mixing between direct input of rainfall through the karstic system and leaching of soil / sediment derived nitrogen. The $\delta^{15}N_{NO_3}$ values of cave waters are similar to those found in the soils/sediments. The dilute nature of nitrate within rainfall, and the limited range of nitrogen isotopic composition between sources suggests cave waters are diluted to intermediate concentrations whilst retaining an isotopic composition dominated by signatures of soil mineralisation and nitrification. Due to the dominant influence of soil mineralisation and nitrification in the system, there is also an almost complete absence of ammonia in the cave waters. The difference in $\delta^{15}N_{NO_3}$ composition between the two cave chambers (Figure 3), likely reflects the source of nitrogen subsequently undergoing soil mineralisation and nitrification. Intensively managed pasture above High Hopes Chamber, with application of farmyard slurry /

409 manure, delivers a cave water nitrate isotopic signature enriched in ^{15}N. Rough grazing on the steep hillside above
410 Whoopee Hall, with minimal influence from farmyard slurry / manure application produces a cave water $\delta^{15}N_{NO_3}$
411 relatively depleted in ^{15}N.

412 The oxygen isotopic composition of nitrate within cave drip waters provides information on the presence of
413 biogeochemical cycling and the relative contribution of rainfall derived inputs. The measured $\delta^{18}O_{NO_3}$ within
414 incoming rainfall has values typical of those reported in the literature when analysed using the same microbial
415 denitrifier method (~+60‰ to +95‰, Kendall et al., 2007). However, there is a large shift in isotopic composition
416 between input rainfall and cave drip waters. Nitrate-oxygen isotopic values of cave waters range between -2.5‰
417 to +6.0‰. If nitrification is the sole pathway for the production of nitrate within the cave system, this should
418 produce a dripwater $\delta^{18}O_{NO_3}$ value that ranges between -15.0‰ to -1.9‰, assuming the following conditions: a
419 1:2 stoichiometry of atmospheric O_2 and rainfall oxygen incorporation into newly formed nitrate molecules;
420 assumed values of +23.5‰ for atmospheric O_2 (Kroopnick and Craig, 1972); a measured rainfall $\delta^{18}O_{H_2O}$ range of
421 +0.2‰ to -11.2‰ within the Matienzo-Riaño region between 2011-2019; and experimentally derived
422 fractionation factors during ammonia oxidation (Casciotti et al., 2010) and oxidation of nitrite to nitrate
423 (Buchwald and Casciotti 2010). However, dripwater $\delta^{18}O_{NO_3}$ signatures from both chambers exceed that expected
424 when assuming nitrification to be the sole production pathway (Figure 3). Where dripwater $\delta^{18}O_{NO_3}$ exceeds the
425 upper limit of this range, further fractionation or mixing with additional nitrate source materials may be invoked.
426 In the present cave environmental setting where redox conditions are well-oxygenated and microbial
427 denitrification is deemed not to be present, we consider mixing with rainfall-derived (atmospheric) nitrate
428 enriched in ^{18}O to be responsible for the excursion of values above the maximum calculated threshold.

429

430 This partial direct transit of nutrients into cave systems has also been observed as part of the sulphur
431 biogeochemical cycle, where either excessive atmospheric deposition of pollutant derived sulphur enabled a
432 direct transfer into the cave dripwaters under a diminished significance of biogeochemical cycling (Wynn et al.,
433 2013), or an ephemeral fracture flow system allowed the rapid transport of meteoric water through the karst
434 with limited storage and mixing en-route. Even though all drip sites at Cueva-cubío del Llanío in both High Hopes
435 Chamber and Whoopee Hall are well-homogenised in both nitrate concentration and isotopic composition,
436 representing a large degree of storage and mixing of water sources within the matrix of the epikarst aquifer, a
437 proportion of fracture flow can be expected after heavy rainfall events. It is thus suspected the origin of the
438 $\delta^{18}O_{NO_3}$ which lies above the calculated threshold value for nitrification, are due to a proportion of meteoric
439 water being delivered to the drip sites according to site specific karst hydrological characteristics. The proportion
440 of sources contributing to drip waters within each cave chamber has been parameterised using a Bayesian
441 isotope mixing model (Table 4). Within High Hopes chamber, drips fed from ephemeral fracture pathways
442 (labelled 'Fast drips 1 and 2 in Table 1), comprise 49.8% (5.4% 1SD) of nitrate sourced from manure, whilst the re-
443 mineralisation of fixed N_2 and/or the nitrification of rainfall-derived ammonia contributes 36.6% (5.4% 1SD) and
444 the remaining signal 13.6% (0.9% 1 SD) is derived from the direct contribution of nitrate contained within rainfall.
445 Within the same chamber, drip sites fed by a matrix-controlled hydrological pathway (High Hopes drips 1-6)
446 support a greater proportion of nitrate sourced from the direct contribution of rainfall (16.1%, 0.8% 1SD). In the
447 cave waters from Whoopee Hall, cave waters fed from ephemeral fracture pathways (Whoopee pool) comprise
448 just 33% (5% 1SD) of nitrate sourced from manure, whilst 54.9% (5.1% 1SD) of nitrate is sourced from the re-
449 mineralisation of fixed N_2 and/or the nitrification of rainfall-derived ammonia, and 12.2% (1.1% 1SD) sourced
450 from the direct entry of rainfall derived nitrate. Matrix-controlled pathways within Whoopee Hall (Whoopee Drip)
451 contain 14.7% (1.3% 1SD) of nitrate derived from the direct entry of rainfall. Mixing models thus support the
452 contention that cave waters in High Hopes chamber convey a greater proportion of nitrate sourced from manure.
453 They also demonstrate cave waters fed by ephemeral or fracture flow characteristics contain a lower proportion
454 of nitrate sourced from the direct entry of rainfall, thus indicating fracture pathways to convey a greater
455 proportion of water which is sourced from the base of the soil zone, compared to matrix-fed drips within the
456 same chamber. It is therefore the nutrient status of the cave surface ecosystem, aswell as the nature of the land

surface inputs and cave system hydrology that work in concert to drive the isotopic composition of the product dripwaters. Input management, soil biogeochemical processing and Epikarst hydrology, thus all appear to be controlling agents of dripwater nitrate composition.

5.2 Transfer of drip water nitrate into the speleothem record at Cueva-cubío del Llanío

The concentration and isotopic composition of nitrate within speleothem calcite has great potential to inform on past groundwater nitrate dynamics. However, this is dependent upon nitrate partitioning and isotopic fractionation between cave drip water and associated speleothem carbonate being quantified.

The nitrate concentrations contained within modern speleothem carbonates from Cueva-cubío del Llanío range between 0.05 to 0.37 mM NO_3. Partitioning between dripwater and speleothem carbonate causes an offset in the nitrate concentration between aqueous to solid phase. Field based partition coefficients are calculated and presented within Table 2. Values of DNO_3 (x 10^{-5}) represent a relative efficiency of incorporation into contemporary speleothem calcite, ranging between 0.06 to 0.42 for the replacement of carbonate with nitrate, with no percieved difference between cave chambers. Compared to the partitioning of sulphate into calcite (Wynn et al., 2018), where the mechanism of incorporation is assumed to follow similar principles of anion substitution (Kontrec et al., 2004), the nitrate molecule represents a lower efficiency of incorporation by approximately 1-3 orders of magnitude (Note the typographical error in Wynn et al., 2018 where all DSO_4 values are given as x10^{5}, instead of x10^{-5}). Quantifying the efficiency of nitrate incorporation into speleothem calcite is an essential first step in enabling semi-quantitative reconstruction of former nitrate loading to karst vadose zone groundwater. While the mechanism of incorporation of nitrate into calcite is unresolved, we note that the thermochemical radii of the CO_3^{2-} ion (0.178 nm) and NO_3^- (0.179 nm) are similar. Given this alone, we would expect the NO_3^- to readily substitute for the CO_3^{2-} on lattice sites of calcite. However, any substitutions must maintain overall electroneutrality i.e. balance of formal charges for the constituent ions within the crystal. The substitution of NO_3^- therefore requires a concurrent substitution of the Ca^{2+} cation by a monovalent cation. Of the alkali halides, Na^+ and Li^+ offer the highest possibility as their radii are either comparable (Na^+) or smaller (Li^+) than that of Ca^{2+} (ionic radii: Ca^{2+} 0.100 nm; Li^+ 0.760; Na^+ 0.102 nm; K^+ 0.138 nm) (Wiredchemist, 2021). The availability of the monovalent ion in the aqueous environment is therefore expected to influence the extent of substitution as reflected by the partition coefficient DNO_3, and indeed may explain, to some extent, the variation in these values. Further, the partition coefficient values have a thermodynamic basis and are unlikely to define the prevailing supersaturation of NO_3^- when calcite is being deposited. Clearly, fundamental studies are required to characterise the $NO_3^- - CO_3^{2-}$ substitution in calcite.

The isotopic composition of contemporary speleothem carbonate grown on glass plates beneath active drip sites within Cueva-cubío del Llanío is presented in Figure 3 and Table 2. Values of $\delta^{15}N_{NO_3}$ contained within speleothem carbonate reflect closely those found within the associated cave drip waters (Figure 3). This suggests there is little fractionation of $\delta^{15}N_{NO_3}$ during the incorporation of nitrate into calcium carbonate and that time-resolved records of speleothem carbonate would make excellent archives of changing groundwater nitrogen source. However, values of $\delta^{18}O_{NO_3}$ contained within speleothem carbonate appear to be of intermediate value to those found in the drip waters and input rainfall. This enrichment in nitrate ^{18}O compared to the counterpart drip waters could be due to fractionation either in the laboratory or on the speleothem surface, or due to the time-integrated nature of carbonate deposition (6 months duration) relative to shorter drip water collection times (approx. 24 hours at the drip sites of concern). Fractionation in the laboratory during sample processing would typically occur during acid digestion of carbonate, whereby nitrate ions may undergo equilibrium isotopic exchange with the ambient water (Kaneko and Poulson, 2013). However, despite the acidic pH during carbonate digestion, such isotopic exchange is considered too slow at the low reaction temperature (room temperature) and the short timescale of low pH conditions (the reaction between carbonate powder and hydrochloric acid proceeds to completion to achieve a neutral pH). Fractionation on the speleothem surface could be induced if the presence of nitrate assimilating bacteria specific to the cave environment caused further biogeochemical cycling and thus

fractionation of nitrate isotopes away from those found within the drip waters. However, if speleothem surface microbes were responsible for driving isotopic enrichment in nitrate ^{18}O via assimilation, this enrichment would also be expected within the cave pool waters, which contain drip waters after transit across the speleothem surface and cave floor. The similarity of $\delta^{18}O_{NO_3}$ within both drip and pool waters would seem to negate this effect. We therefore consider the time-integrated nature of speleothem carbonate deposition (6 months) relative to drip water collection (24 hours at the drip sites of concern) to be the main contributing factor to nitrate ^{18}O enrichment. Over a growth period of 6 months, carbonate deposition will integrate dripwater nitrate sourced predominantly from the well-mixed groundwater store, sporadically over-printed by short lived fracture flow events during rainfall, delivering atmospheric nitrate enriched in ^{18}O which hasn't undergone any prior biogeochemical modification in the soil and epikarst. Bayesian mixing models parameterise the proportion of rainfall nitrate in contemporary speleothem calcite to range between 31.1% (4.7% 1 SD) for Whoopee Hall to 42.1% (2.7% 1SD) of the total nitrate signature in High Hopes chamber (Table 4).

5.3. Transfer of drip water nitrate into speleothem records from other cave sites

Nitrate concentrations and isotopes extracted from speleothems grown in cave sites where intensive nitrogen biogeochemical monitoring of the contemporary system has not been undertaken, are used to demonstrate the ubiquitous presence of nitrate within speleothem carbonate and its utility in resolving the nitrogen status of the formation drip/vadose zone water. Nitrate concentration, $\delta^{15}N_{NO_3}$ and $\delta^{18}O_{NO_3}$ was extracted from the outer growth layers of archived speleothem samples collected from Browns Folly Mine, Somerset, UK (Baker et al., 1998) and Merc-1, Ethiopia (Baker et al., 2007; Asrat et al., 2008), or from modern carbonate precipitate collected on glass plates beneath active drip sites at Cueva de las Perlas, Matienzo, N. Spain (Deeprose, 2018) and Pooles Cavern, Derbyshire, UK. Material of indeterminate age (albeit certainly pre-anthropogenic) was also drilled from the base of speleothem Ease Gill 1, Yorkshire Dales, UK (Table 3). Concentrations of nitrate present within speleothem calcite depict a broad range (0.02 to 0.86 mM), with the greatest concentrations present within Ethiopian sample (Merc-1). Where concentrations of nitrate have been monitored in both drip waters and coeval speleothem calcite, values of DNO_3 are calculated. These are presented as $DNO_3^{x10\text{-}5}$ = 0.11 for Merc-1 and $DNO_3^{x10\text{-}5}$ = 0.45 for Cueva de las Perlas (Table 2). Efficiency of nitrate incorporation into speleothem calcite thus appears to be within a similar range of values to those observed within Cueva-cubío del Llanío, confirming the utility of DNO_3 beyond an individual set of cave environmental conditions. The data presented (Figure 4) depict a narrow range of $\delta^{15}N_{NO_3}$ values, but a range of $\delta^{18}O_{NO_3}$ which is broader than that discovered in Cueva-cubío del Llanío, N. Spain. Speleothem Ease Gill-1 supports nitrate sourced from a dominant rainfall end-member. The pre-anthropogenic calcite sourced from the base of this formation precludes the presence of inorganic fertilisers and extensive manure sources. Both $\delta^{15}N_{NO_3}$ and $\delta^{18}ONO_3$ therefore place the nitrate source firmly as atmospheric deposition, which enters into the cave system without any biogeochemical cycling to re-set the oxygen isotopic value. Speleothem Merc-1, from Rukiesa cave, Mechara, Ethiopia, supports a $\delta^{15}N_{NO_3}$ isotopic composition which places the nitrogen source at the boundary between manure and inorganic fertiliser. The $\delta^{18}O_{NO_3}$ signatures from two separate drill aliquots range from +6.0 to +14.5‰. The intensively cultivated area above the caves and greatest concentration of nitrate recorded in speleothem calcite to date (Table 3) would seem to support an inorganic ammonia and nitrate fertilizer origin), with the former being mineralised prior to incorporation into the stalagmite calcite. A proportion of atmospheric nitrate entering into the cave without prior biogeochemical modification is consistent with $\delta^{18}O_{NO_3}$ above the maximum calculated threshold for nitrification and a fracture flow component delivering meteoric water observed at this site (Asrat et al., 2008). Other speleothem samples tested (Cueva de las Perlas, Matienzo, N. Spain; Pooles Cavern, Derbyshire, UK; Browns Folly Mine, Somerset, UK) all represent modern deposition within cave sites beneath scrubland with low intensity grazing, or woodland established within the last 100 years. The $\delta^{15}N_{NO_3}$ values of all three sites fall within the overlapping source range of rainfall, manure-N and inorganic ammonia fertiliser. The overlying vegetation would largely preclude any organic or inorganic fertiliser input, suggesting a natural soil derived nitrogen, ultimately derived from atmospheric deposition and nitrogen fixation to be the main source of nitrogen in drip waters and speleothem

calcite. Values of $\delta^{18}O_{NO_3}$ in the same samples lie beyond the expected range for microbial nitrification, suggesting a proportion of nitrogen deposition must be as atmospheric nitrate which enters directly into the cave drip waters without prior biogeochemical modification in the soil zone.

Speleothem carbonate thus seems to reflect the isotopic composition of vadose zone nitrate, but which demands the dual isotopic analysis of $\delta^{15}N_{NO_3}$ and $\delta^{18}O_{NO_3}$ to enable both source and biogeochemical modification to be detected. As atmospheric nitrate also supports a mass independent excess of ^{17}O over that expected from ^{18}O ($\Delta^{17}O$) (eg. Michalski et al., 2003), which is inherited through atmospheric reaction with ozone, we propose the use of nitrate $\Delta^{17}O$ in addition to $\delta^{15}N$ and $\delta^{18}O$ as a tracer of atmospheric nitrate deposition entering into the cave / groundwater system without prior biogeochemical modification (cf. Dietzel et al., 2014).

Conclusions

The potential for speleothem carbonate to accurately record signals of vadose zone nitrate which extend prior to the era of groundwater monitoring is dependent upon understanding the impact of biogeochemical cycling, karst hydrological dynamics and partitioning, upon signal integrity. Within cave waters, measurements of $\delta^{15}N_{NO_3}$ demonstrate source characteristics of input nitrogen to be well preserved throughout the soil and epikarst biogeochemical cycle. Values of $\delta^{18}O_{NO_3}$ within dripwaters provide a deeper insight into biogeochemical processing and hydrological dynamics, highlighting the importance of atmospheric nitrate deposition entering directly through the karst without prior biogeochemical modification. Both biogeochemical cycling and hydrological dynamics work in concert to determine the characteristics of dripwater nitrate entering into the cave system. Across the dripwater-contemporary carbonate interface, partitioning controls the concentration of nitrate incorporated into the speleothem record in a quantifiable manner and the speleothem isotopic record seems unaffected by fractionation between phases. $\delta^{15}N_{NO_3}$ within speleothem carbonate is thus deemed an excellent indicator of source, whilst $\delta^{18}O_{NO_3}$ within carbonate provides a sensitive indicator of karst hydrological dynamics and biogeochemical processing. On the basis of nitrate isotope systematics established within contemporary speleothem calcite, application to age-constrained records which extend throughout the anthropogenic era promise an exciting development in the ability to trace vadose zone pollution dynamics. Of specific interest is the ability to establish a baseline pollution status to contextualise current levels of nitrate inputs, to determine nitrate retention (legacy) dynamics through the direct comparison of input records and speleothem concentration profiles, and the opportunity to trace inputs to source using stable isotopes. Parameterisation of vadose zone nitrate dynamics in this way is also important for the refinement of karst hydrological models which are currently in a limited state of development for the prediction of nitrate groundwater quality within karst.

Figures

Figure 1: Cave plan for Cueva-cubío del Llanío, Matienzo, N. Spain.

Figure 2: Nitrogen concentration and isotope composition of cave waters, rainfall and soil/sediment in the Cueva-cubío del Llanío system.

Figure 3: Nitrate isotope composition of cave waters, rainfall and contemporary speleothem calcite in Cueva-cubío del Llanío.

Boxes defining the expected range of values for $\delta^{15}N_{NO_3}$ obtained from the mineralisation/nitrification of manure, inorganic fertiliser and rainfall ammonia are sourced from Kendall et al. (2007). The range in $\delta^{15}N_{NO_3}$ expected from rainfall represent those values obtained only through the microbial denitrifier method (Kendall et al., 2007). The expected range in $\delta^{15}N_{NO_3}$ obtained from the re-mineralisation and nitrification of Fixed N_2 is presented assuming minimal fractionation from source organic matter. The expected range in $\delta^{18}O_{NO_3}$ values obtained

during mineralisation/nitrification have been calculated using fractionation factors developed through Casciotti et al., 2007, Casciotti et al., 2010, Casciotti and Buchwald, 2010, and values of rainfall $\delta^{18}O_{H_2O}$ specific to Matienzo between 2011-2019 (see data repository for full compilation of values).

Figure 4: Nitrate isotope composition of speleothem calcite deposited within shallow cave systems beneath contrasting surface vegetation characteristics.

Boxes defining the expected range of values for $\delta^{15}N_{NO_3}$ obtained from the mineralisation/nitrification of manure, inorganic fertiliser and rainfall ammonia are sourced from Kendall et al. (2007). The range in $\delta^{15}N_{NO_3}$ expected from rainfall represent those values obtained only through the microbial denitrifier method (Kendall et al., 2007). The expected range in $\delta^{15}N_{NO_3}$ obtained from the re-mineralisation and nitrification of Fixed N_2 is presented assuming minimal fractionation from source organic matter. The expected range in $\delta^{18}O_{NO_3}$ values obtained during mineralisation/nitrification have been calculated using fractionation factors developed through Casciotti et al., 2007, Casciotti et al., 2010, Casciotti and Buchwald, 2010, and values of rainfall $\delta^{18}O_{H_2O}$ specific to each cave site. For cave sites in the Matienzo locale, rainfall $\delta^{18}O_{H_2O}$ specific to Matienzo between 2011-2019 have been used. For Rukiesa cave, Ethiopia, rainfall $\delta^{18}O_{H_2O}$ was obtained from the Global Network of Isotopes in Precipitation (GNIP) database for Addis Ababa between 1961 to 2016. For UK cave sites, rainfall $\delta^{18}O_{H_2O}$ was obtained from the GNIP database for Wallingford, UK between 1979 to 2015 (IAEA/WMO, 2020).

Figure S1: Rainfall and drip water discharge records at Cueva-cubío del Llanío, collected between January 2018 to September 2019.

Figure S2: Monthly water excess between January 2018 to September 2019 for the Cueva-cubío del Llanío region.

Tables

Table 1: Summary data for cave waters, rainfall, soils/sediments and vegetation at Cueva-cubío del Llanío.

Table 2: Calculated partition co-eficients between cave waters and speleothem calcite at Cueva-cubío del Llanío.

Table 3: Nitrate isotope characteristics of speleothem deposits growing within cave systems which support a variety of surface vegetation characteristics.

Table 4: Summary modelling statistics (Mean ± 1SD) for Bayesian isotope mixing (MixSIAR) presented as proportional contributions (%) of nitrate sources into cave water and contemporary speleothem deposits. Nitrate sources include (1) manure nitrate, (2) Nitrification of rainfall ammonia and/or re-mineralisation of fixed N_2, and (3) direct input of rainfall nitrate.

Data availability

The underlying data pertaining to figures and tables is available from http://dx.doi.org/10.17635/lancaster/researchdata/xxx.

Declaration of interests

The authors declare no known competing financial interests.

Acknowledgements

This work was supported by the UK Natural Environment Research Council (NERC) National Environmental Isotope Facility (NEIF) (Grant LSMSF\CEH\L\125\11\2018), and Lancaster University. Thanks are expressed to Dr. A Smith of the British Geological Survey, the British Cave Research Association Cave Science Centre and the staff at Pooles Cavern, UK for enabling access to the cave and allowing monitoring activities to be undertaken. Access to speleothem samples previously collected from Browns Folly Mine, UK and Rukiesa Cave, Ethiopia was obtained with kind permission from Prof. A. Baker (University of New South Wales, Australia), and Prof. A. Asrat (Addis Ababa University, Ethiopia). We are also grateful for the kind permission from Dr. Laura Deeprose (formerly of Lancaster University) to use cave monitoring data and modern speleothem calcite collected as a part of her unpublished doctorate research thesis. Mr. D. Hughes is thanked for his work in the Lancaster Environment Centre Stable Isotope Laboratory. The Cantabrian government and the Matienzo caves Project provided access to the cave site and provided invaluable assistance with logistical support and sample collection, for which we are extremely grateful.

Bibliography

Aranburu, A., Arriolabengoa, M., Iriarte, E., Giralt, S., Yusta, I., Martínez-Pillado, V ., Val, M. Moreno, J. and Jimenez-Sanchez, M. 2015. Karst landscape evolution in the littoral area of the Bay of Biscay (north Iberian Peninsula). Quaternary International, 364, 217-230. Doi: 10.1016/j.quaint.2014.09.025

Ascott, M.J., Goody, D.C., Wang, L., Stuart, M.E., Lewis, M.A., Ward, R.S. and Binley, A.M. 2017. Global patterns of nitrate storage in the vadose zone. Nature Communications, 8, 1416. Doi: 10.1038/s41467-017-01321-w

Asrat A., Baker A., Umer MM., Leng MJ., Van Calsteren., P. and Smith C. 2007. A high-resolution multi-proxy stalagmite record from Mechara, Southeastern Ethiopia: palaeohydrological implications for speleothem palaeoclimate reconstruction. Journal of Quaternary Science, 22, 53–63. Doi: 10.1002/jqs.1013

Asrat, A., Baker, A., Leng, M.J., Gunn, J. and Umer, M. 2008. Environmental monitoring in the Mechara caves, Southeastern Ethiopia: implications for speleothem palaeoclimate studies. International Journal of Speleology, 37 (3) 207-220.

Baker, A., Genty, D., Dreybodt, W., Barnes, W., Mockler, N and Grapes, J. (1998) Testing theoretically predicted stalagmite growth rate with recently annually laminated samples: Implications for past stalagmite deposition. Geochimica et Cosmochimica Acta, 62, 393-404.

Baker, A. and Genty, D. 1999. Fluorescence wavelength and intensity variations of cave waters. Journal of Hydrology, 217, 19-34.

Baker, A., Mockler, N., and Barnes, W. 1999a. Fluorescence intensity variations of speleothem forming groundwaters: Implications for paleoclimate reconstruction. *Water Resources Research*, 35, 407-413.

Baker, A, Proctor, C J and Barnes, W L, 1999b. Variations in stalagmite luminescence laminae structure at Poole's Cavern, England, AD 1910–1996: calibration of a palaeoprecipitation proxy. Holocene, Vol.9, 683–688.

Baker, A., Asrat, A., Fairchild, IJ., Leng, M.J., Wynn, P.M., Bryant, C. Genty, D. and Umer, M. (2007) Analysis of the climate signal contained within $\delta^{18}O$ and growth rate parameters in two Ethiopian stalagmites. Geochimica et Cosmochimica Acta. 71, 2975-2988. Doi:10.1016/j.gca.2007.03.029

683 Baldini, J. (2001) Morphological and dimensional linkage between recently deposited speleothems and drip water
684 from Browns Folly Mine, Wiltshire, England. Journal of Cave and Karst Studies, 63: 83-90.
685
686 Baldini, J.U.L, McDermott, F., Baker, A., Baldini, L.M., Mattey, D.P and Railsback., L.B. (2005) Biomass effects on
687 stalagmite growth and isotope ratios: A 20th century analogue from Wiltshire, England. Earth and Planetary
688 Science Letters, 240, 486-494. Doi: 10.1016/j.epsl.2005.09.022
689
690 Buchwald, C. and Casciotti, K.L. 2010. Oxygen isotopic fractionation and exchange during bacterial nitrite
691 oxidation. Limnology and Oceanography, 55 (3) 1064-1074. doi:10.4319/lo.2010.55.3.1064
692
693 Cameron, K.C., Di, H.J. and Moir, J.L. 2013. Nitrogen losses from the soil/plant system: a review. Annals of Applied
694 Biology, 162, 145-173. doi:10.1111/aab.12014
695
696 Casciotti, K.L., Sigman, D.M., Hastings, M.G., Böhlke, J.K. and Hilkert, A. 2002. Measurement of the oxygen
697 isotopic composition of nitrate in seawater and freshwater using the denitrifier method. Annals of Chemistry, 74,
698 4905-4912. Doi: 10.1021/ac020113w
699
700 Casciotti, K.L., Sigman, D.L. and Ward, B.B. 2003. Linking Diversity and Stable Isotope Fractionation in Ammonia-
701 Oxidizing Bacteria, Geomicrobiology Journal, 20:4, 335-353. Doi: 10.1080/01490450390241035
702
703 Casciotti, K.L., Böhlke, J.K., McIlvin, M.R., Mroczkowski, S.J. and Hannon, J.E. 2007. Oxygen Isotopes in Nitrite:
704 Analysis, Calibration, and Equilibration. Annals of chemistry, 79, 2427-2436. Doi: 10.1021/ac061598h
705
706 Casciotti, K.L. 2009. Inverse kinetic isotope fractionation during bacterial nitrite oxidation. Geochimica et
707 Cosmochimica Acta, 73, 2061- 2076. Doi:10.1016/j.gca.2008.12.022
708
709 Casciotti, K.L., McIlvin, M., and Buchwald, C. 2010. Oxygen isotopic exchange and fractionation during bacterial
710 ammonia oxidation. Limnology and Oceanography, 55 (2) 753-762.
711
712 Chalk, P.M., Inácio, C.T. and Chen, D. 2019. An overview of contemporary advances in the usage of 15N natural
713 abundance ($\delta^{15}N$) as a tracer of agro-ecosystem N cycle processes that impact the environment. Agriculture,
714 Ecosystems and Environment, 283, 106570. Doi: 10.1016/j.agee.2019.106570
715
716 Deeprose, L.M.C. 2018. *Speleothem Climate Capture of the Neanderthal demise.* PhD, Lancaster University.
717
718 Dewit, J., Foubert, A., Desouky, H.A., Muchez, P., Hunt, D., Vanhaecke, F. and Swennen, R. 2014. Characteristics,
719 genesis and parameters controlling the development of a large stratabound HTD body at Matienzo (Ramales
720 Platform, Basque-Cantabrian Basin, northern Spain). Marine and petroleum Geology, 55, 6-25. Doi:
721 10.1016/j.marpetgeo.2013.12.021
722
723 Dietzel, M., Leis, A., Abdalla, R., Savarino, J., Morin, S, Böttcher, M.E. and Köhler, S. 2014. ^{17}O excess traces
724 atmospheric nitrate in paleo-groundwater of the Saharan desert. Biogeosciences, 11, 3149- 3161.
725 Doi:10.5194/bg-11-3149-2014
726
727 Evans, D.R. 2001. Physiological mechanisms influencing plant nitrogen isotope composition. Trends in plant
728 science, 6 (3)
729
730 Fairchild, I.J., Tuckwell, G.W., Baker, A and Tooth, A.F. 2006. Modelling of drip water hydrology and
731 hydrogeochemistry in a weakly karstified aquifer (Bath, UK): Implications for climate change studies. *Journal of*
732 *Hydrology*, **321**, 213-231. Doi:10.1016/j.jhydrol.2005.08.002
733

734 Fairchild, I.J. and Treble, P.C. 2009. Trace elements in speleothems as recorders of environmental change.
735 Quaternary Science Reviews, 28, 449-468. Doi: 10.1016/j.quascirev.2008.11.007
736
737 Ford, D.C and Williams, P. Karst Hydrogeology and geomorphology. Wiley (2013).
738
739 Galloway, J.N., Townsend, A.R., Erisman, J.W., Bekunda, M., Cai, Z.C., Freney. J.R., Martinelli, L.A., Seitzinger, S.P.
740 and Sutton, M.A. 2008. Transformation of the nitrogen cycle: Recent trends, questions, and potential solutions.
741 Science, 320, 889-892.
742
743 Galloway, J.N., Townsend, A.R., Erisman, J.W., Bekunda, M., Cai, Z., Freney, J.R., Martinelli, L.A., Seitzinger, S.P.
744 and Sutton, M.A. 2008. Transformation of the nitrogen cycle: Recent trends, questions, and potential solutions.
745 Science, 320 (5878) 889-892. Doi: 10.1126/science.1136674**.**
746
747 Gutiérrez, J. 2010. Geological map of Matienzo, Arredondo, Ogarrio and surroundings. *In:* Corrin, J., and Smith, P.
748 (eds.) *Matienzo 50 years of speleology.* Bacup: Matienzo Caves.
749
750 Hartland, A., Fairchild, I.J., Lead, J.R., Borsato, A., Baker, A., Frisia, S., Baalousha, M. 2012. From soil to cave:
751 transport of trace metals by natural organic matter in karst drip waters. *Chem. Geol.*, **304**, 68-82. Doi:
752 10.1016/j.chemgeo.2012.01.032
753
754 Hartland A., Fairchild, I.J., Lead. J.R., Zhang, H. and Baalousha, M. 2011. Size, speciation and lability of NOM-metal
755 complexes in hyperalkaline cave dripwater. Geochimica et Cosmochimica Acta, 75, 7533-7551
756
757 Hartland, A., Fairchild, I.J., Lead, J.R., Dominguez-Villar, D., Baker, SA., Gunn, J., Baalousha, M. and Ju-Nam, Y.
758 2010. The dripwaters and speleothems of Poole's Cavern: A review of recent and ongoing research. Cave and
759 Karst Science, 36 (2) 37-46.
760
761 Heaton, T. H. E. 1986. Isotopic studies of nitrogen pollution in the hydrosphere and atmosphere: a review.
762 Chemical Geology, 59, 87-102.
763
764 Högberg, P. 1997. Tansley Review No. 95. 15N natural abundance in soil-plant systems. New Phytologist, 137,
765 179-203
766
767 Husic, A., Fox, J., Adams, E., Backus, J., Pollock,E., Ford, W. and Agourdis, C. 2019a. Inland impacts of atmospheric
768 river and tropical cyclone extremes on nitrate transport and stable isotope measurements. Environmental Earth
769 Sciences. 78:36. Doi: 10.1007/s12665-018-8018-x
770
771 Husic, A., Fox, J., Adams, E., Ford, W., Agourdis, C., Currens, J. and Backus, J. 2019b. Nitrate Pathways, Processes,
772 and Timing in an Agricultural Karst System: Development and Application of a Numerical Model. Water Resources
773 Research, 55, 2079-2103. Doi: 10.1029/2018WR023703
774
775 Jiménez-Sánchez, M., Stoll, H., Vadillo, I., López-Chicano, M., Domínguez-Cuesta, M., Martín-Rosalez, W. and
776 Meléndez-Asensio, M. 2008. Groundwater contamination in caves: four case studies In Spain. International
777 Journal of Speleology, 37 (1) 53-66.
778
779 Kaneko, M. and Poulson, S.R. 2013. The rate of oxygen isotope exchange between nitrate and water. Geochimica
780 et Cosmochimica Acta, 118, 148-156. Doi: 10.1016/j.gca.2013.05.010
781
782 Kendall, C., Elliot, E.M. and Wankel, S.D. 2007. Tracing anthropogenic inputs of nitrogen to ecosystems. In:
783 Michener, R.H. and Lajtha, K. (eds.) Stable isotopes in ecology and environmental science. 2nd edition. Blackwell
784 publishing, p. 375-449.

Kontrec, J., Kralj, D., Brecˇevi c´, L., Falini, G., Fermani, S., Noethig-Laslo, V. and Mirosavljevi c´, K. 2004. Incorporation of inorganic anions in calcite. European Journal of Inorganic Chemistry, 4579-4585. Doi: 10.1002/ejic.200400268

Kroopnick, P.M. and Craig, H.C. 1972. Atospheric oxygen: isotopic compsotion and solubility fractionation. Science, 175 (4017) 54-55. Doi: 10.1126/science.175.4017.54

Liu, X-Y., Koba, K., Makabe, A. and Liu, C-Q. 2014. Nitrate dynamics in natural plants: insights based on the concentration and natural isotope abundances of tissue nitrate. Frontiers in plant science, 5, article number 355. Doi: 10.3389/fpls.2014.00355

Matiatos, I., Wassenaar, L.I., Monteiro, L.R., Venkiteswaran, J.J., Gooddy, D,C., Boeckx, P., Sacchi, E., Yue, F-J., Michalski, G., Alonso-Hernández, C., Biasi, C., Bouchaou, L., Edirisinghi, N.V., Fadhullah, W., Fianko, J.R., García-Moya, A., Kazakis, N., Li, S-L., Luu, M.T.N., Priyadarshanee, S., Re, V., Rivera, D.S., Romanelli, A., Sanyal, P., Tamooh, F., Trinh, D.A., Walters, W., and Welti, N. 2021. Global patterns of nitrate isotope composition in rivers and adjacent aquifers reveal reactive nitrogen cascading. Communications Earth and Environment.

Mayer B, Bollwerk SM, Mansfeldt T, Hütter B, Veizer J. 2001. The oxygen isotope composition of nitrate generated by nitrification in acid forest floors. Geochimica et Cosmochimica Acta, 65, 2743–2756. Doi.org/10.1016/S0016-7037(01)00612-3

Michalski, G., Scott, Z., Kabiling, M and Thiemens, M.H. 2003. First measurements and modelling of $\delta^{17}O$ in atmospheric nitrate *Geophysical research letters*, 30 (16), art. No-1870. Doi: 10.1029/2003GL017015

Newton, K.E., Fairchild, IJ. and Gunn, J. 2015. Rates of calcite precipitation from hyperalkaline waters, Poole's Cavern, Derbyshire, UK. Cave and Karst Science, 42 (3) 116-124.

Romanelli, A., Soto, D.X., Matiatos, I., Martínez, D.E., Esquius, S. 2020. A biological and nitrate isotopic assessment framework to understand eutrophication in aquatic ecosystems. Science of The Total Environment, 715, 136909. Doi: 10.1016/j.scitotenv.2020.136909

Sigman, D.M., Casciotti, K.L., Andreani, M., Barford, C., Galanter, M. and Böhlke, J.K. 2001. A bacterial method for the nitrogen isotopic analysis of nitrate in seawater and freshwater. Annals of Chemistry, 73, 4145-4153. Doi: 10.1021/ac010088e

Smith, A.C., Wynn, P.M., Barker, P.A. and Leng, M.J. 2015. Drip water electrical conductivity as an indicator of cave ventilation at the event scale. Science of the total environment, 532, 517-527. Doi: 10.1016/j.scitotenv.2015.06.037

Smith, A.C., Wynn, P.M., Barker, P.A., Leng, M.J., Noble, S.R. and Tych, W. 2016a. North Atlantic forcing of moisture delivery to Europe throughout the Holocene. Scientific Reports, 6, 24745. Doi: 10.1038/srep24745

Smith, A.C., Wynn, P.M., Barker, P.A., Leng, M.J., Noble, S.R. and Stott, A. 2016b. Cave monitoring and the potential for palaeoclimate reconstruction from Cueva de Asiul, Cantabria (N. Spain). International Journal of Speleology, 45 (1), 1-9. Doi: 10.5038/1827-806X.45.1.1928

Soto, D.X., Koehler, G., Wassenaar, L.I., Hobson, K.A. 2019. Spatio-temporal variation of nitrate sources to Lake Winnipeg using N and O isotope ($\delta^{15}N$, $\delta^{18}O$) analyses. Sci. Total Environ., 647, 486–493. Doi: 10.1016/j.scitotenv.2018.07.346

Stock, B.C., Semmens, B.X. 2013. MixSIAR User Manual. Version 3.1. https://github.com/brianstock/MixSIAR.

Venkiteswaran, J.J., Boeckx, P., Gooddy, D.C. 2019. Towards a global interpretation of dual nitrate isotopes in surface waters. Journal of Hydrology X, 4, 100037. Doi: 10.1016/j.hydroa.2019.100037

Vitousek, P.M., Aber, J.D., Howarth, R.W., Likens, G.E., Matson, P.A., Schindler, D.W., Schlesinger, W.H. and Tilman, D.G. 1997. Technical report: Human alteration of the global nitrogen cycle: Sources and consequences. *Ecological Applications,* 7 (3), 737-750.

Wang, L., Butcher, A.S., Stuart, M.E., Gooddy, D.C. and Bloomfield, J.C. 2013. The nitrate time bomb: A numerical way to investigate nitrate storage and lag time in the unsaturated zone. Environ. Geochem. Health, 35, 667-681. Doi: 10.1007/s10653-013-9550-y

Wells, N.S., Baisden, W.T. and Clough, T.J. 2015. Ammonia volatilisation is not the dominant factor in determining the soil nitrate isotopic composition of pasture systems. Agriculture, Ecosystems and Environment, 199, 290-300. Doi: 10.1016/j.agee.2014.10.001

Wynn, P.M., Fairchild, I.J., Baker, A., Baldini, J.U.L. and McDermott, F. 2008. Isotopic archives of sulphate in speleothems. *Geochim. Cosmochim. Acta* **72**, 2465-2477. Doi:10.1016/j.gca.2008.03.002

Wynn, P.M., Borsato, A., Baker, A., Frisia, S., Miorandi, R. & Fairchild, I.J. 2013. Biogeochemical cycling of sulphur in karst and transfer into speleothem archives at Grotta di Ernesto, Italy. *Biogeochemistry* **114**, 255-267. Doi: 10.1007/s10533-012-9807-z

Wynn, P.M., Fairchild, I.J., Borsato, A., Spötl, C., Hartland, A., Baker, A., Frisia, S. and Baldini, J.U.L. 2018. Sulphate partitioning into calcite: Experimental verification of pH control and application to seasonality in speleothems. Geochimica et Cosmochimica Acta, 226, 69-83. Doi: 10.1016/j.gca.2018.01.020

Yang, P., Wang, Y., Wu, X., Chang, L., Ham, B., Song, L. and Groves, C. 2020. Nitrate sources and biogeochemical processes in karst underground rivers impacted by different anthropogenic input characteristics. Environmental Pollution, 265, 114835. Doi: 0.1016/j.envpol.2020.114835

Yue, F-J., Li, S-L., Zhong, J. and Liu, J. 2018. Evaluation of Factors Driving Seasonal Nitrate Variations in Surface and Underground Systems of a Karst Catchment. Vadose Zone Journal. 17:170071. Doi:10.2136/vzj2017.04.0071

Yue, F-J, Waldron, S., Li, S-L., Wang, Z-J., Zeng, J., Xu, S., Zhang, Z-C. and Oliver, D.M. 2019. Land use interacts with changes in catchment hydrology to generate chronic nitrate pollution in karst waters and strong seasonality in excess nitrate export. Science of the Total Environment, 696, 134062. Doi: 10.1016/j.scitotenv.2019.134062

Internet source references

http://www.wiredchemist.com/chemistry/data/atomic-and-ionic-radii (accessed 6th August 2020).

[Dataset] IAEA/WMO (2020). Global Network of Isotopes in Precipitation. The GNIP Database. Accessible at: http://www.iaea.org/water (accessed 8th July 2020).

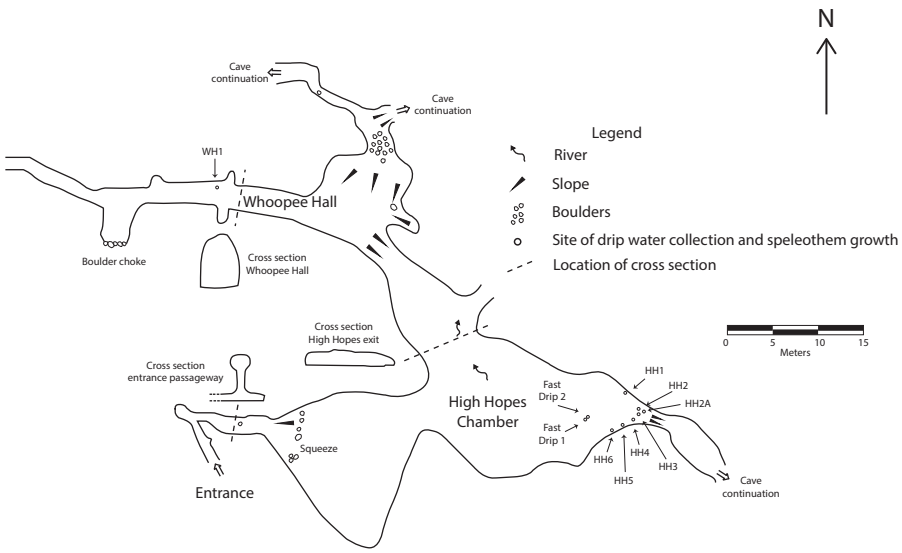
N
Cave continuation
Cave continuation
WH1
Whoopee Hall
Boulder choke
Cross section Whoopee Hall
Cross section High Hopes exit
Cross section entrance passageway
Squeeze
Entrance
High Hopes Chamber
Fast Drip 2
Fast Drip 1
HH1
HH2
HH2A
HH6
HH4
HH5
HH3
Cave continuation
Legend
River
Slope
Boulders
Site of drip water collection and speleothem growth
Location of cross section
0
5
10
15
Meters

Figure 2

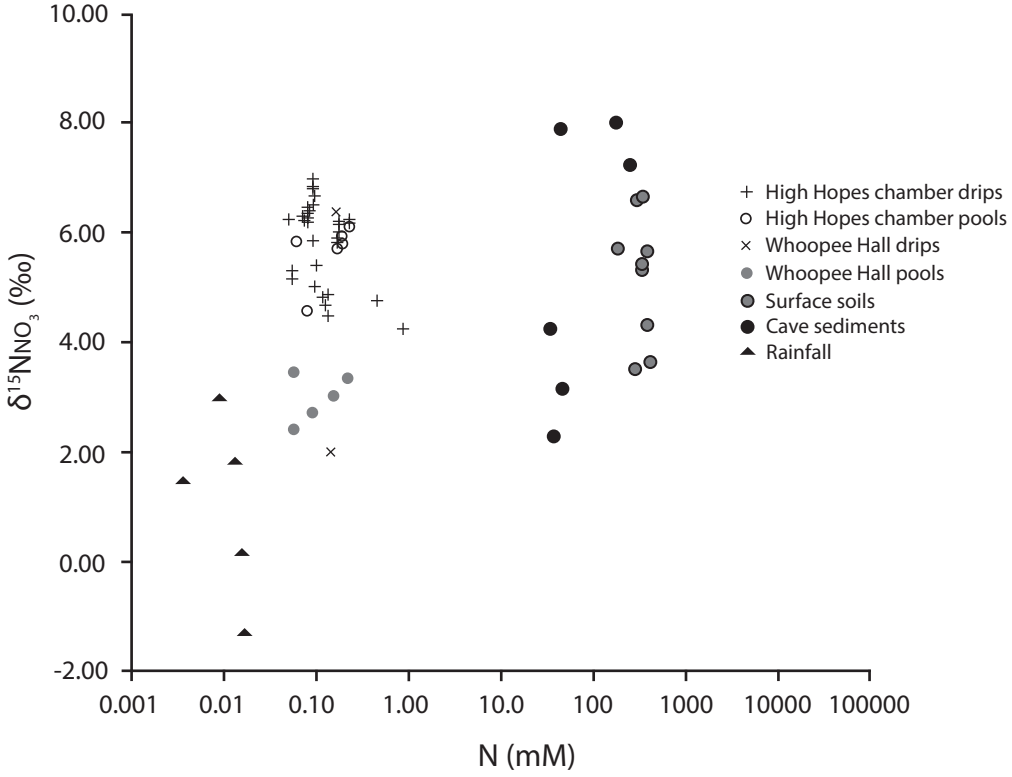
10.00
8.00
6.00
4.00
2.00
0.00
-2.00
δ15NNO3 (‰)
0.001
0.01
0.10
1.00
10.0
100
1000
10000
100000
N (mM)
High Hopes chamber drips
High Hopes chamber pools
Whoopee Hall drips
Whoopee Hall pools
Surface soils
Cave sediments
Rainfall

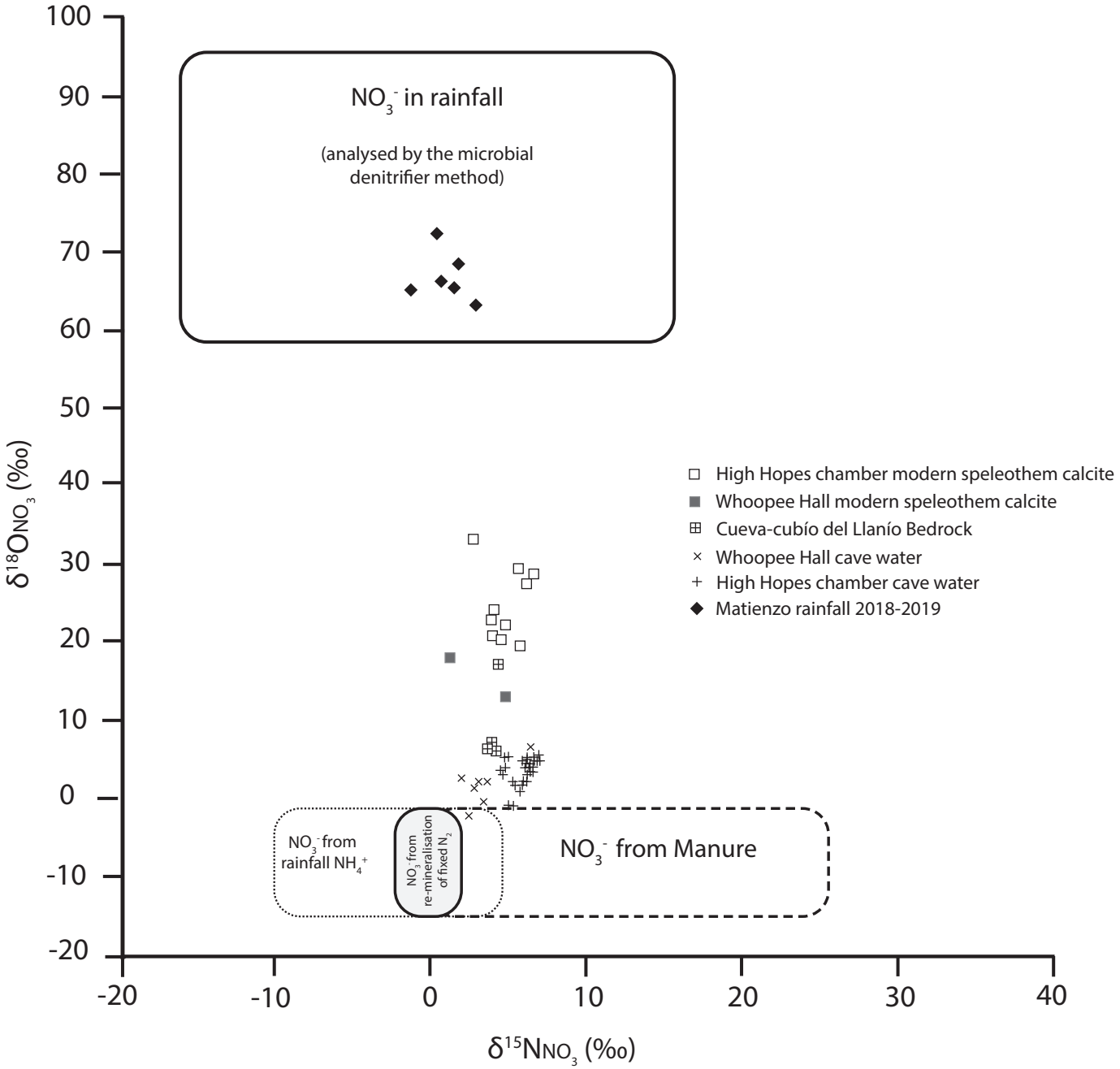
100
90
80
70
60
50
40
30
20
10
0
-10
-20
-20
-10
0
10
20
30
40
δ18ONO3 (‰)
δ15NNO3 (‰)
NO3- in rainfall
(analysed by the microbial denitrifier method)
High Hopes chamber modern speleothem calcite
Whoopee Hall modern speleothem calcite
Cueva-cubío del Llanío Bedrock
Whoopee Hall cave water
High Hopes chamber cave water
Matienzo rainfall 2018-2019
NO3- from rainfall NH4+
NO3- from re-mineralisation of fixed N2
NO3- from Manure

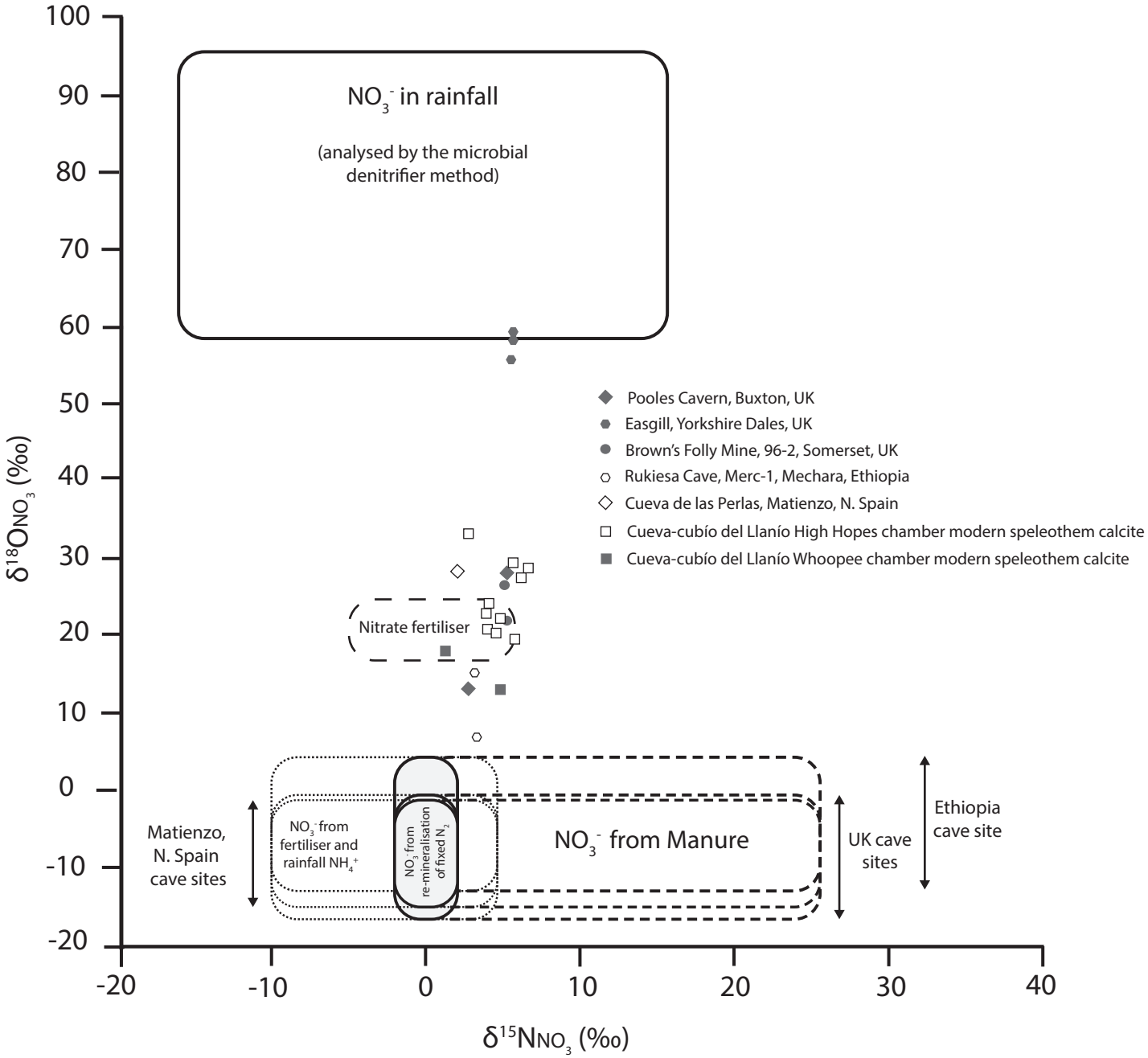
100
90
80
70
60
50
40
30
20
10
0
-10
-20
-20
-10
0
10
20
30
40
δ18ONO3 (‰)
δ15NNO3 (‰)
NO3- in rainfall
(analysed by the microbial denitrifier method)
Pooles Cavern, Buxton, UK
Easgill, Yorkshire Dales, UK
Brown's Folly Mine, 96-2, Somerset, UK
Rukiesa Cave, Merc-1, Mechara, Ethiopia
Cueva de las Perlas, Matienzo, N. Spain
Cueva-cubío del Llanío High Hopes chamber modern speleothem calcite
Cueva-cubío del Llanío Whoopee chamber modern speleothem calcite
Nitrate fertiliser
Matienzo, N. Spain cave sites
NO3- from fertiliser and rainfall NH4+
NO3- from re-mineralisation of fixed N2
NO3- from Manure
UK cave sites
Ethiopia cave site

885

886

887

888

889

890

891

892 Table 1

Sample	pH	EC	Temp (°C)	Total alkalinity (mM $CaCO_3$)	NO_3-N (mM)	NH_4-N (mM)	$\delta^{15}NNO_3$ (‰)	$\delta^{18}ONO_3$ (‰)
Dripwaters								
High Hopes Fast Drip 1	7.46	390	12.8	1.80	0.15	0.009	+6.0	+2.2
	n = 2	n = 2	n = 2	n = 1	n = 6	n = 1	n = 5	n = 5
	(7.14 to 7.78)	(384 to 395)	(12.5 to 13.0)		(0.05 to 0.23)		(+5.3 to +6.2)	(-1.3 to +4.7)
High Hopes Fast Drip 2	7.85	384.00	12.70	1.50	0.17	0.002	+5.9	+2.1
	n = 1	n = 1	n = 1	n = 2	n = 5	n = 1	n = 4	n = 4
				(1.24 to 1.76)	(0.05 to 0.23)		(+5.2 to +6.2)	(-1.5 to +4.4)
High Hopes 1	7.86	493	14.6	No data available	0.12	0.007	+4.7	+3.5
	n = 1	n = 2	n = 1		n = 6	n = 3	n = 4	n = 4
		(455 to 531)			(0.10 to 0.13)	(0.002 to 0.011)	(+4.5 to +4.9)	(+2.8 to +4.7)
High Hopes 2	7.97	460	12.4	1.93	0.09	0.005	+6.4	+4.0
	n = 4	n = 4	n = 3	n = 3	n = 4	n = 2	n = 5	n = 5
	(7.59 to 8.16)	(435 to 479)	(11.4 to 14.3)	(1.64 to 2.40)	(0.08 to 0.09)	(0.005 to 0.005)	(+5.3 to +7.0)	(+1.5 to +4.5)
High Hopes 2A	7.79	448	13.3	1.84	0.08	0.011	+6.5	+3.9
	n = 2	n = 3	n = 2	n = 1	n = 3	n = 2	n = 3	n = 3
	(7.62 to 7.95)	(444 to 455)	(11.8 to 14.7)		(0.08 to 0.09)	(0.004 to 0.017)	(+6.2 to +6.8)	(+3.4 to +4.8)
High Hopes 3	7.96	441	14.4	1.59	0.09	0.005	+5.9	+2.7
	n = 2	n = 3	n = 1	n = 2	n = 3	n = 2	n = 3	n = 3
	(7.87 to 8.05)	(425 to 461)		(1.48 to 1.70)	(0.08 to 0.11)	(0.005 to 0.005)	(+5.4 to +6.2)	(+1.2 to +3.5)
High Hopes 4	8.03	446	12.5	1.87	0.09	0.006	+6.1	+3.8
	n = 3	n = 4	n = 3	n = 3	n = 4	n = 2	n = 4	n = 4
	7.84 to 8.14	(435 to 458)	(11.5 to 14.2)	(1.85 to 1.88)	(0.07 to 0.10)	(0.005 to 0.008)	(+5.0 to +6.8)	(+2.8 to +4.9)
High Hopes 5	7.87	437	14.1	No data available	0.09	0.004	+6.5	+3.4
	n = 1	n = 2	n = 1		n = 3	n = 2	n = 3	n =3
		(436 to 437)			(0.08 to 0.09)	(0.004 to 0.004)	(+6.4 to +6.8)	(+2.9 to +4.5)
High Hopes 6	8.00	436	13.0	1.88	0.09	0.004	+6.5	+4.0
	n = 2	n = 3	n = 2	n = 2	n = 3	n = 3	n = 3	n = 3
	(7.88 to 8.11)	(417 to 455)	(12.1 to 13.8)	(1.80 to 1.96)	(0.09 to 0.10)	(0.004 to 0.005)	(+6.3 to +6.6)	(+3.4 to +4.7)
Whoopee Hall 1	8.18	386	11.7	1.53	0.15	<LOD	+4.2	+4.2

	n = 2 (8.17 to 8.20)	n = 2 (359 to 413)	n = 1	n = 2 (1.40 to 1.66)	n = 2 (0.14 to 0.17)		n = 2 (+2.0 to +6.4)	n = 2 (+2.4 to +6.0)
Pool waters								
High Hopes Pools	8.10 n = 4 7.87 to 8.20	365 n = 5 (344 to 382)	11.8 n = 5 (11.4 to 13.0)	1.69 n = 5 (1.64 to 1.82)	0.17 n = 6 (0.06 to 0.23)	0.011 n = 1	+5.9 n = 6 (+5.8 to +6.1)	+1.7 n = 6 (+0.3 to +3.8)
Whoopee Hall Pools	7.99 n = 3 (7.89 to 8.11)	347 n = 5 (278 to 427)	13.7 n = 3 (12.4 to 14.4)	1.30 n = 2 (1.25 to 1.36)	0.12 n = 5 (0.06 to 0.23)	0.006 n = 4 (0.004 to 0.008)	+3.0 n = 5 (+2.4 to +3.4)	+1.3 n = 5 (-2.5 to +1.9)
Rain water								
Jan – April, Sept 2019	---	31 n = 3 (28.0 to 70.0)	---	---	0.01 n = 7 (0.001 to 0.02)	0.012 n = 7 (0.006 to 0.021)	+1.0 n = 5 (-1.3 to +3.0)	+66.5 n = 5 (+62.3 to +71.9)
Vegetation								
At cave entrance	---	---	---	---	2148 n = 3 (2110 to 2170)	---	+0.3 n = 3 (-1.1 to +1.0)	---
Above Hope chamber	---	---	---	---	2012 n = 3 (1555 to 2599)	---	+1.4 n = 3 (+0.4 to +2.3)	---
Soils / sediments								
Hope chamber Surface soils	---	---	---	---	327 n = 6 (196 to 364)	---	+5.9 n = 6 (+5.4 to +6.7)	---
Whoopee chamber Surface soils	---	---	---	---	404.8 n = 3 (319.1 to 461.9)		+3.8 n = 3 (+3.5 to +4.2)	---
Cave sediments	---	---	---	---	72.9 n = 5 (35.7 to 192.9)	---	+5.1 n = 5 (+2.3 to +8.0)	---
Bedrocks								
Llanio bedrock	---	---	---	---	0.71 n = 2 (0.5 to 0.9)	---	+4.5 n = 2 (+4.2 to +4.7)	10.81 n = 2 (+5.4 to +16.2)

Tabulated data are presented as average values, with the data range presented in parentheses. n-values vary with sample site and measurement parameter, due to site specific conditions impacting sampling frequency and availability of water for chemical determinands. Underlying data to tabulated summary statistics is available through the data repository at http://dx.doi.org/10.17635/lancaster/researchdata/xxx.

Table 2

Speleothem growth site	Collection interval	Growth substrate	Dripwater pH[a]	Water Temperature (°C)[a]	Dripwater CO_3^{2-} (mM)[b]	Dripwater HCO_3^- (mM)[b]	Dripwater NO_3^- (mM)[c]	Dripwater NO_3^-/CO_3^{2-} molar ratio[d]	NO_3^- (mM) speleothem calcite[e]	NO_3^-/CO_3^{2-} speleothem calcite[f]	$DNO3_{CO3}$ ($^{x\ 10-5}$)[g]	$\delta^{15}NNO_3$ speleo (‰)[h]	$\delta^{18}ONO_3$ speleo (‰)[h]
Hope Chamber 2	January 2019 – August 2019	Stalagmate surface	7.93 n = 3 (7.59 to 8.16)	12.4 n = 3 (11.4 to 14.3)	0.020 n = 2 (0.015 to 0.027)	4.12 n = 2 (3.49 to 4.75)	0.09 n = 4 (0.08 to 0.09)	4.24 (3.42 to 5.34)	0.1 n = 1	9.98^{x10-6}	0.24 (0.19 to 0.29)	+6.1 n = 1	+18.9 n = 1
Hope Chamber 3	January 2018 – January 2019	Stalagmate surface	8.05 n = 1	No data	0.013 n = 1	2.93 n = 1	0.11 n = 1	8.3	0.08 n = 4 (0.05 to 0.11)	7.56^{x10-6} (4.77^{x10-6} to 1.13^{x10-5})	0.09 (0.06 to 0.14)	+4.6 n = 4 (+4.3 to +5.3)	+21.0 n = 4 (+20.0 to +22.3)
Hope Chamber 3	January 2019 – September 2019	Watch glass	7.87 n = 1	14.4 n = 1	0.011 n = 1	3.38 n = 1	0.08 n = 2 (0.08 to 0.09)	7.79 (7.50 to 8.07)	0.15 n = 1	1.46^{x10-5}	0.19 (0.18 to 0.20)	+6.4 n = 1	+27.0 n = 1
Hope Chamber 4	January 2019 – September 2019	Watch glass	8.03 n = 3 (7.84 to 8.14)	12.5 n = 3 (11.5 to 14.2)	0.016 n = 3 (0.011 to 0.020)	3.71 n = 3 (3.68 to 3.72)	0.09 n = 4 (0.07 to 0.10)	5.38 (4.76 to 6.73)	0.12 n = 1	1.23^{x10-5}	0.23 (0.18 to 0.26)	+4.4 n = 1	+23.2 n = 1
Hope Chamber 6	January 2019 – September 2019	Watch glass	8.00 n = 2 (7.88 to 8.11)	13.0 n = 2 (12.1 to 13.8)	0.015 n = 1	3.73 n = 1	0.09 n = 3 (0.09 to 0.10)	6.17 (5.60 to 6.51)	0.12 n = 1	1.21^{x10-5}	0.20 (0.19 to 0.22)	+3.3 n = 1	+32.3 n = 1
Whoopee Chamber 1	January 2018 – January 2019	Stalagmate surface	8.18 n = 2 (8.17 to 8.20)	11.7 n = 1	0.018 n = 2 (0.016 to 0.02)	3.02 n = 2 (2.77 to 3.28)	0.15 n = 2 (0.14 to 0.17)	8.67 (8.19 to 8.98)	0.08 n = 1	8.05^{x10-6}	0.09 (0.09 to 0.10)	+1.6 n = 1	+17.2 n = 1
Whoopee Chamber 1	January 2019 – August 2019	Stalagmate surface	8.17 n = 1	11.7 n = 1	0.016 n = 1	2.77 n = 1	0.14 n = 1	8.98	0.37 n = 1	3.74^{x10-5}	0.42	+5.1 n = 1	+12.3 n = 1

Merc-1 Rukiesa, Ethiopia[i]	2004	Speleothem latest growth	7.81 n = 8 (7.47 to 8.15)	No data	0.022 n = 11 (0.002 to 0.089)	6.17 n = 11 (1.55 to 10.7)	1.77 n = 2 (0.71 to 2.83)	79.2 (31.7 to 300.3)	0.85 (0.841 to 0.859)	8.497^{x10-5} (8.41^{x10-5} to 8.59^{x10-5})	0.11 (0.03 to 0.27)	+3.5 (+3.5 to +3.6) n = 2	+10.2 (+6.0 to +14.5) n = 2
CP1-15 Perlas, Matienzo[j]	2013-2015	Watch glass	8.39 n = 12 (8.1 to 8.52)	13.4 n = 12 (12.0 to 14.8)	0.027 n = 3 (0.012 to 0.039)	2.71 n = 3 (2.57 to 2.77)	0.04 n = 4 (0.006 to 0.088)	1.47 (0.46 to 2.30)	0.07 n = 1	6.63^{x10-6}	0.45 (0.29 to 1.43)	+2.1 n = 1	+28.2 n = 1

Tabulated data are presented as average values, with the data range presented in parentheses. See data repository for underlying analytical results. n-values vary with sample site and measurement parameter, due to site specific conditions impacting sampling frequency and availability of water for chemical determinands.

[a]Range in Temp and pH reflect measured value

[b]Total inorganic carbon speciation was undertaken using PHREEQC and concentrations derived from relative activity co-efficients. The range in carbonate and bicarbonate values reflects measured alkalinity and associated sample pH unless otherwise stated.

[c]Range in nitrate represents true sample values

[d]Range in NO_3^-/CO_3^{2-} ratio in drip waters reflects pairing of max and min values in each data set.

[e]Range in speleothem nitrate represents replicate analyses of the same sample

[f]Range in NO_3^-/CO_3^{2-} ratio of speleothem calcite represents replicate analyses of the same sample.

[g]Range in $DNO3^{x10-5}$ represents pairing of max and min solid and solution ratios for each sample.

[h]Range in speleothem isotope values represents replicate analyses of the same sample.

[i]pH data taken from Asrat et al., (2008). Carbonate and bicarbonate values calculated from calcium and magnesium data obtained from Asrat et al., (2008).

[j]All raw data obtained from Deeprose (2018).

Table 3

Speleothem Name	Cave details	Sample description	Year of calcite deposition	NO_3 (mM) in speleothem carbonate	$\delta^{15}N_{NO_3}$ (‰) speleothem carbonate	$\delta^{18}O_{NO_3}$ (‰) speleothem carbonate	n =	References
MERC-1	Rukiesa cave, Ethiopia, Mercury chamber	Speleothem (surface scrape). Actively depositing when collected. Natural cave site developed within Jurassic Limestone, intercalated with marl and mudstone. Cave chamber 25 m below the surface. Overlying vegetation comprises agricultural cultivation of maize and millet following woodland clearance in the 1930's	2004	0.850 (0.841 to 0.859)	+3.5 (+3.5 to +3.6)	+10.2 (+6.0 to +14.5)	2	Asrat et al., 2007, 2008; Baker et al., 2007
BFM-96-2	Browns Folly Mine, UK	Speleothem (surface scrape). Actively depositing when collected. Building stone mine within Oolitic limestone, Somerset, UK. Mine abandoned in 1886. Overlying secondary woodland developed over the past 100 years.	1996	0.086 (0.081 to 0.090)	+5.5 (+5.4 to +5.5)	+23.6 (+21.2 to +25.9)	2	Baker et al., 1998, 1999; Baldini et al., 2001, 2005; Fairchild et al., 2006
Perlas CP1-15	Cueva Perlas, Matienzo, N. Spain	Calcite deposition on watch glass. Natural cave site with approx. 7 m overburden rock thickness, formed in a hydrothermal dolomite body within Early Cretaceous carbonate deposits. The cave site is overlain by natural grassland supporting low intensity grazing.	2013-2015	0.066	+2.1	+28.2	1	Deeprose, L. 2018
Pooles RC1	Pooles Cavern, Derbyshire, UK. Roman Chamber	Calcite deposition on watch glass beneath hyperalkaline drip site (pH = 12). Natural cave site overlain by limewaste from early 20th C activity. Deciduous woodland forms vegetation cover since at least 1820.	June 2019	0.047	+3.1	+13.5	1	Baker and Genty, 1999; Baker et al., 1999b; Hartland et al., 2010, 2012; Newton et al., 2015
Pooles PE2	Pooles Cavern, Derbyshire, UK. Poached Egg chamber	Calcite deposition on watch glass beneath hyperalkaline drip site (pH = 10-11). Natural cave site overlain by limewaste from early 20th C activity. Deciduous woodland forms vegetation cover since at least 1820.	June 2019	0.021	+5.3	+28.4	1	Baker et al., 1998b; Baker and Genty, 1999; Hartland et al., 2010, 2012; Newton et al., 2015
Ease Gill 1	Ease Gill caverns, Cumbria, UK	Speleothem (basal drill sample). Collected in Ease Gill Beck, abandoned away from site of growth. Natural cave site formed within Lower carboniferous limestone on the Yorkshire Dales – Cumbrian border. Overlying vegetation is natural grassland supporting low intensity rough grazing.	Pre-anthropogenic	0.186 (0.181 to 0.191)	+6.0 (+5.8 to +6.0)	+57.3 (+55.3 to +58.6)	3	No publications to date

Data values are presented as analytical averages, with ranges presented in parentheses.

Number of analyses (n =) refers to separate drill aliquots extracted from each speleothem, other than Ease Gill 1 where n represents repeat analysis of a bulk extracted powder.

Table 4

Cave Chamber	Cave water Type	Manure	Nitrification	Rainfall
High Hopes (n=15)	Fracture	49.8 ± 5.4	36.6 ± 5.4	13.6 ± 0.9
High Hopes (n=25)	Matrix	51.0 ± 5.5	32.9 ± 5.5	16.1 ± 0.8
Whoopee Hall (n=5)	Fracture	33.0 ± 5.0	54.9 ± 5.1	12.2 ± 1.1
Whoopee Hall (n=2)	Matrix	34.8 ± 5.6	50.5 ± 5.8	14.7 ± 1.3
High Hopes speleothem (n=5)	Matrix	36.2 ± 5.4	21.7 ± 5.7	42.1 ± 2.7
Whoopee Hall speleothem (n=2)	Matrix	33.3 ± 10.9	35.6 ± 11.3	31.1 ± 4.7

Supplementary information

Contemporary systematics of vadose zone nitrate capture by speleothem carbonate

Wynn P.M[a*]., Ambler, S[a]., Grefe I[a]., Soto D.X[b]., Surridge, B.W.J[a]., Gabitov, R.I[c]., Barker, P.A[a]., Anwar, J[a]., Quin, A[a]., Pereira, M.G[b]. and Grant H.K[b]

[a]*Lancaster Environment Centre, Lancaster University, Lancaster,*

LA1 4YQ, UK.

[b] *UK Centre for Ecology and Hydrology, Lancaster, LA1 4AP, UK*

[c]*Department of Geosciences, Mississippi State University, Mississippi State, MS 39762, United States.*

Corresponding author. E-mail address: p.wynn@lancaster.ac.uk

Drip rate and rainfall intensity data from Cueva-cubío del Llanío

Drip rates were monitored in Cueva-cubío del Llanío using stalagmate loggers placed on top of actively depositing speleothems. Each logging device was programmed to record the number of drips every 10 mins, with data processed to represent drip discharge in millilitres per hour. The conversion from drip count to water volume assumed a volume of 0.1 ml per drop (Collister and Mattey, 2008). Rainfall was recorded using a Pluvimate logger and raingauge housing, sited in the neighbouring village of Matienzo. Rainfall was recorded as drops per 10 mins, converted to mm per hour using the conversion factor of 0.012. The record duration from each logger was dependent upon the battery life and memory capacity of each device, hence the logging hiatus between September 2018 to January 2019. Temperature was monitored external to the cave system in the neighbouring village of Matienzo, using a Tinytag Plus, TGP4017. Data were logged at one hour intervals and have an accuracy of +/- 0.01 °C.

Figure S1 presents a rainfall record collected between January 2018 to September 2019 within the neighbouring village of Matienzo, plotted against the drip rate response of three separate drip locations within Cueva-cubío del Llanío. The rainfall record shows a seasonal distribution, with maxima occurring during the winter and minima during the summer months. This distribution is consistent with more extensive records within the region (Smith et al., 2016; Deeprose et al., 2018).

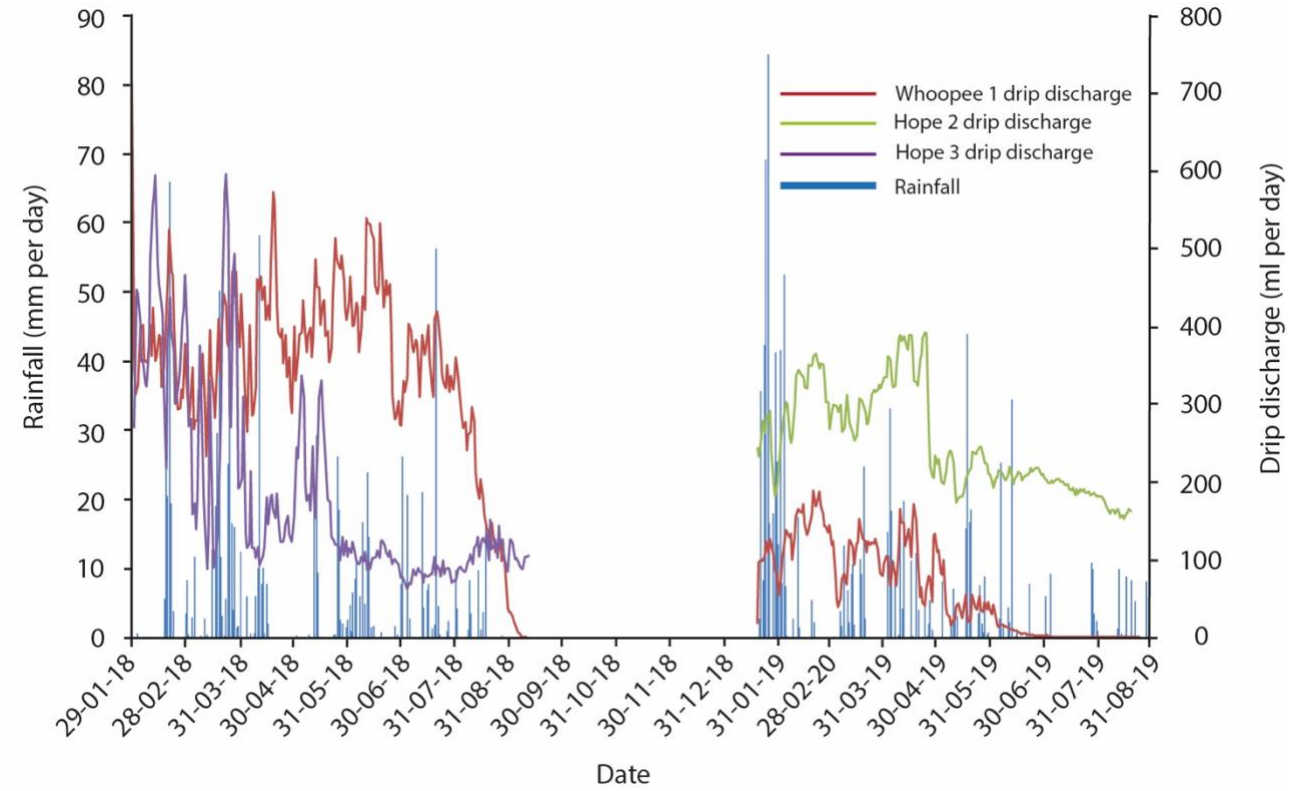

Figure S1: Rainfall and drip water discharge records at Cueva-cubío del Llanío, collected between January 2018 to September 2019.

Monthly water excess (Figure S2) (calculated following Thornthwaite et al., 1948) is recognised to be in deficit within the region between June to September (Smith et al., 2016). Within Whoopee Chamber

(Cueva-cubío del Llaníο), drip rate diminishes towards flow cessation in response to the annual period of negative water excess. Flow cessation indicates drip water supply from an aquifer of limited volume within the karst. This is consistent with the limited rock overburden (5 m thickness) at this site. Drip records from Hope chamber demonstrate a more persistent flux of water into the cave, achieving minimal values during the summer months, albeit never reaching flow cessation within the duration of the logged period. Whilst all drip records are responsive to external winter rainfall events, the most dramatic excursions are apparent within High hopes chamber, suggesting a greater degree of flow path connectivity through the karst and with the surface. This degree of responsiveness diminishes during the summer months as the negative water excess prevents replenishment of the karst aquifer. Drip rate records within High Hopes Chamber are thus consistent with a well-connected karst network, fed by an aquifer of sufficient volume to enable active dripping throughout the period of negative water excess. Within Whoopee Hall, the aquifer demonstrates poorer connectivity to external rainfall events, but is of limited volume such that flow cessation occurs during the summer months of negative water excess.

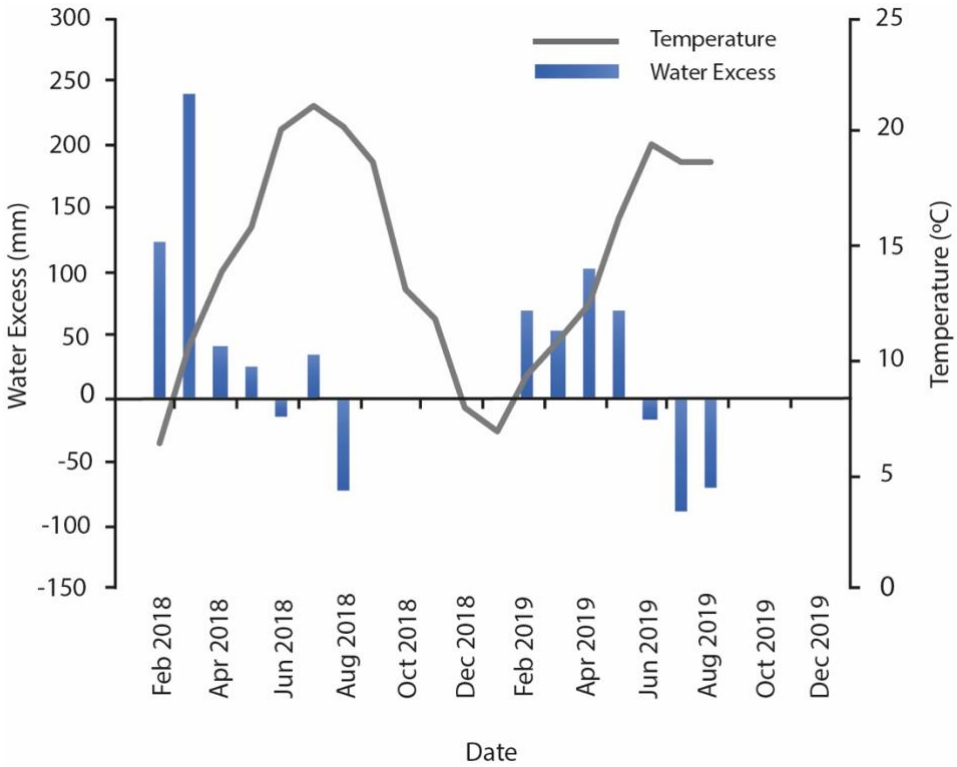

Figure S2: Monthly water excess between January 2018 to September 2019 for the Cueva-cubío del Llaníο region.

References

Collister, C. and Mattey, D. 2008. Controls on water drop volume at speleothem drip sites: An experimental study. Journal of Hydrology, 358, 259-267.

Deeprose, L.M.C 2018. *Speleothem Climate Capture of the Neanderthal demise.* PhD, Lancaster University.

Smith, A.C., Wynn, P.M., Barker, P.A., Leng, M.J., Noble, S.R. and Stott, A. 2016. Cave monitoring and the potential for palaeoclimate reconstruction from Cueva de Asiul, Cantabria (N. Spain). International Journal of Speleology, 45 (1), 1-9.

THORNTHWAITE, C. W. 1948. An approach toward a rational classification of climate. *Geographical review,* 38**,** 55-94.